Aircraft Design for AIAA Design Build Fly Competition

A Major Qualifying Project Report
Submitted to the Faculty of the
WORCESTER POLYTECHNIC INSTITUTE
in Partial Fulfillment of the Requirements for the
Degree of Bachelor of Science
in Aerospace Engineering

by

Christopher Davenport

Jordan Jonas

Joshua Martin

Harrison Mazur

Samuel Vinson

Bridget Wirtz

April 28, 2022

Approved by:

Zhangxian Yuan, Advisor

Professor, Aerospace Engineering Department

WPI

David Olinger, Co-Advisor

Professor, Aerospace Engineering Department

WPI

Abstract

The goal of this MQP was to design, build, and fly a radio-controlled aircraft that meets the 2022 AIAA DBF competition design and flight requirements. The objective of this competition was to produce an aircraft to complete humanitarian missions related to the ongoing Covid-19 pandemic. The missions included the deployment of the aircraft, storing of vaccination syringes, and delivery of environmentally sensitive vaccine vial packages. There were four missions total: one relating to speed, two focused on payload transportation, and another relating to payload loading. The maximum allowed linear dimension of the aircraft was 8 feet, and the aircraft was limited to a maximum battery capacity of 100 watt-hours. The final design configuration included a 5 foot fuselage and a 7.5 foot wingspan. The aircraft carried two vaccine vial packages and more than 20 syringes. During the DBF competition, the team successfully passed one of four missions, surviving 50-60 mph wind gusts and a complete loss of thrust midflight.

Acknowledgements

The Design Build Fly Team would like to thank Professor Yuan for providing us with his immeasurable support and his wealth of knowledge throughout the duration of this MQP. His suggestions and willingness to work with the team throughout the design process was invaluable. The Design Build Fly Team would also like to thank Professor Olinger for his help with training the team how to use the wind tunnel which was used to procure extremely important aerodynamic data throughout the project. Professor Olinger also provided the team with written material from his lecture, Aircraft Design, which proved to be highly useful throughout the course of this project. The team would additionally like to thank the WPI Aerospace Engineering Department, Student Government Association, and the AIAA Student Club for providing travel funds to the AIAA DBF Competition. For assisting in project purchases, the team thanks Tina Stratis and the rest of the Aerospace Department.

Table of Authorship/Work

Section	Work	Writing/Editing
Executive Summary		
Competition Overview	N/a	JM
Design Process	N/a	JM
Final Design	N/a	JM
1 Introduction		
1.1 Project Goals	All	JM
1.2 Project Management	All	All
1.3 MQP Objectives, Methods, and Standards	All	CD
1.4 MQP Timetable & Budget	All	All
2 Conceptual Design		
2.1 Competition Breakdown	All	CD, BW
2.2 Subsystem Design Requirements	All	JM, BW
2.3 Configuration and Component Selection	All	All
3 Preliminary Design		
3.1 Design Methodology	All	All
3.2 Propulsion	CD	CD
3.3 Fuselage	JM, HM	JM, HM
3.4 Aerodynamics	JJ, SV, BW	JJ, SV, BW
4 Detailed Design		
4.1 Dimensional Parameters	All	All
4.2 Structural Characteristics	JM, HM	JM, HM
4.3 Systems Integration & Architecture	All	All
4.4 Overall Aircraft Performance	All	JM, CD
5 Manufacturing		
5.1 Manufacturing Process	All	All
5.2 Manufacturing Process Selection	All	HM, BW
6 Testing Plan		
6.1 Testing Schedule	All	All
6.2 Propulsion Testing	CD	CD
6.3 Structures Testing	HM, JM	HM, JM
6.4 Aerodynamic Testing	JJ, BW	JJ, BW
6.5 Controls Testing	All	SV
6.6 Overall Aircraft Testing	All	All
7 Performance Results		
7.1 Subsystem Performance Results	All	All
8 Aircraft Performance Results		
8.1 Glide Test	All	CD, JM
8.2-5 Flight Test 1 - 5	All	CD, JM
8.6 Final Flight Test Iterations	All	JJ
9 Outcomes & Conclusions		
9.1 Competition Outcomes	All	JJ, BW
9.2 Conclusions	All	JJ, BW
9.3 Broader Impacts	All	CD
9.4 Future Recommendations	All	JJ

Table of Authorship Legend

Initial	Name
CD	Christopher Davenport
JJ	Jordan Jonas
JM	Joshua Martin
HM	Harrison Mazur
SV	Samuel Vinson
BW	Bridget Wirtz

Table of Contents

Table of Figures

Table of Tables

Executive Summary

Competition Overview

This report represents Worcester Polytechnic Institute's 2021-2022 AIAA Design, Build, Fly MQP project. The report details the design, testing, and analysis of a radio-controlled aircraft that meets the AIAA competition design and flight requirements.

The objective of this year's competition was to produce an aircraft to complete humanitarian missions related to the ongoing Covid-19 pandemic. The missions included stable flight of the aircraft, storing of vaccination syringes, and delivery of environmentally sensitive vaccine vial packages. There were four missions total: one relating to speed, two focused on payload transportation, and another relating to payload loading. The maximum allowed linear dimension of the aircraft was 8 feet, and the aircraft was limited to a maximum battery capacity of 100 watt-hours.

To maximize the score, the team prepared a scoring analysis of the DBF competition. This analysis allowed the team to determine the conceptual approach for the design of the aircraft to maximize the score. This led the team to prioritize maximizing the number of syringes that could fit within the fuselage and designing a proper payload deployment system.

Design Process

Stemming from scoring analysis, certain design metrics were utilized to sift through conceptual design configurations. The metrics employed were aerial performance, internal capacity, maneuverability, and manufacturability amongst others. After applying these design metrics, the aerodynamic profile consisted of a high wing, and conventional tail, the fuselage was square with a tail dragger landing gear, and the propulsion system utilized a mono-propeller set up. Within the hollow cabin, the payload bay consisted of an elevator system with string to lower them underneath the underbelly of the aircraft to deploy the vaccine packages. The trapdoors were equipped with servo-operated spool to release slowly dropping the payload to the ground and being able to wind the string back to close the hatch.

Following the determination of the conceptual design of the aircraft, the team then broke into sub-team component design and generated preliminary designs. These preliminary designs then entered the testing phase going through different tests including but not limited to static

thrust testing, wind tunnel testing, XFLR5 simulations, and ANSYS simulations. After completing this stage of testing, the sub-teams then combined all their efforts into a prototype of the aircraft. From this stage on, the team would conduct flight tests, and alter the design to generate new configurations which would improve on certain desired parameters such as take-off distance, stability, total lift, and payload capacity.

Final Design

After performing numerous flight, and take-off tests, the team eventually decided upon a configuration that excelled the team's initial ambitions. Although true, the aircraft suffered numerous mishaps throughout the prototyping phase. The plane flew as a helicopter one flight, wasn't able to sustain flight in another, crashed and burned more than once, and even broke a carbon fiber spar. But with each flight test and mishap, the team understood the aircraft more, and more and eventually found the most balanced configuration for the aircraft.

The final design of aircraft consisted of a single motor monoplane capable of generating 3.3 lbs. of thrust at cruise velocity, 12 pounds of lift, and sustaining a cruise speed of 22.73 ft/s across all three missions. The aircraft utilizes a NACA 4412 airfoil to remain in the skies with a wingspan of 7.5 feet containing ailerons 3.5 inches long, and full span flaps combining the independent flaps, and ailerons for high lift takeoffs. The electronics package consisted of a Scorpion 4020 brushless motor, Scorpion Tribunus II ESC, and various receivers operating the plane, and payload bay which was all powered by a 4 cell 6500mAh LiPo battery. The fuselage of the aircraft was 60 inches long held together by multiple carbon fiber spars, bulkheads, and a lightweight aluminum landing gear.

This aircraft configuration held more than 20 medical syringes, and 2 vaccine vial packages. These were successfully loaded and deployed during the duration of the ground mission. During an attempt of Mission 1, the ESC failed, leading to a loss of thrust. The plane glided to the ground safely to end this team's participation in the DBF competition.

1 Introduction

This project was conducted with two distinct but independent goals: (1) to fulfill the MQP requirements set forth by WPI and (2) to compete and place in the American Institution of Aeronautics and Astronautics (AIAA)'s highly competitive Design, Build, Fly (DBF) competition, advancing both WPI and team members' names within the Aerospace community. The competition provided a unique educational experience where a team of undergraduate students applied years' worth of learning and combined this into a micro aerial vehicle.

1.1 Project Goals

The major goals of the Aircraft Design for AIAA DBF Competitions main goals were as follows:

- Perform the conceptual design of WPI's entry to the AIAA Design, Build, Fly competition which can perform speed and payload based missions. This includes but is not limited to payload delivery of vaccine vial packages, carrying more than 10 medical syringes to a destination, and a high-speed lap.
- Develop prototypes of individual subsystem components for rigorous validation testing.
- Combine successful subsystem components together to form a strong and high quality prototype aircraft which can carry out the missions determined by the competition rules.
- Perform flight tests, validating or invalidating the aircraft's ability to perform, and meet competition requirements. If invalidating, generate design alterations which would enhance the performance of the aircraft.
- Send the final configuration of the aircraft to the AIAA 2022 DBF Competition, and place well within the competition.
- Explore the usage of the aircraft within other domains outside of the competition with a universal payload deployment bay.

1.2 Project Management

To maximize the efficiency of the group members, the team was divided into five groups: structures, propulsion, aerodynamics, controls, and floaters. The structures sub team oversaw the structural analysis, design of the fuselage, payload system and fabrication of the

aircraft. The propulsion sub team researched, selected, and mounted the batteries, motor, and propeller. This required thrust, weight, and drag analysis of the aircraft. The aerodynamics team selected airfoils and completed major aerodynamic analyses. The controls sub team was the most interconnected team, working with each major sub team to integrate appropriately sized control surfaces to work properly with the electronics and wing design put forward by the other teams. There were 10 students in this team in total, four non-senior students were invited to work on this project as per the Design Build Fly Competition Rules. The structures and aerodynamics sub teams each had two members and the propulsion and controls sub teams each had one member. This can be seen in Figure 1 below. There was a total of two freshmen and two juniors who were not assigned to a sub team but were also able to help in any capacity they wanted to.

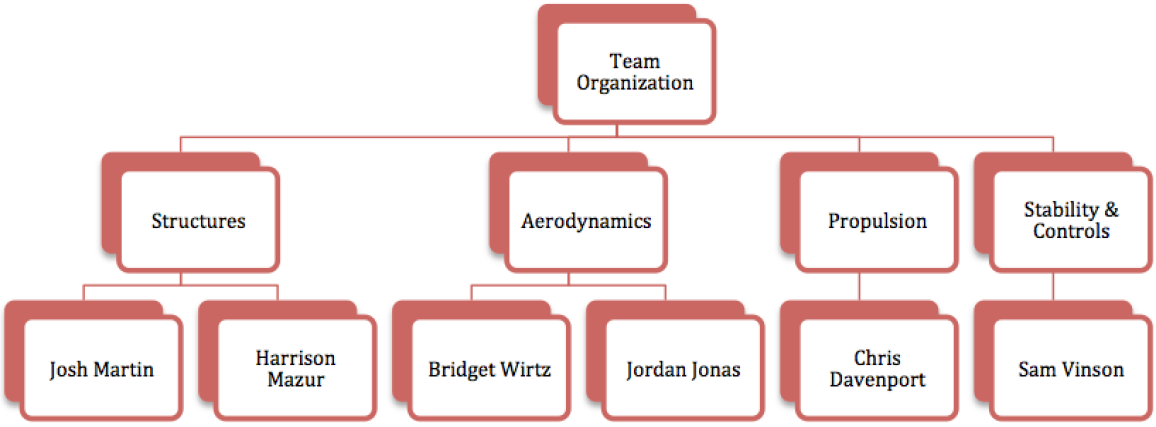

Figure 1: Organization of Sub-teams

The seniors whose names are listed underneath the team organization chart were responsible for the communication as well as the deliverables from that subsystem.

1.3 MQP Objectives, Methods, and Standards

1. Design an aircraft capable of competing in the AIAA Design build Fly Competition
    a. Perform aerodynamic and stability analysis to ensure a stable flight capable of flying all missions. Use XFLR5 to create a model of the aircraft and conduct lift analysis and calculate stability mode eigenvalues.
    b. Analyze the propulsive setup for the aircraft. Use RCBenchmark thrust stand along with the wind tunnel located in HL005 to collect static and dynamic thrust values.

c. Conduct structural analysis of the aircraft and landing gear. Use ANSYS to perform finite element analysis to verify structures.

2. Design a modular payload bay capable of remote deployment of half pound payloads and syringes.
    a. Design a dropping mechanism using SolidWorks that would link with a receiver and be capable of dropping a half pound payload. Dynamic analysis was performed to ensure that 25G shock sensors did not get set off.

1.4 MQP Timetable and Budget

1.4.1 Schedule

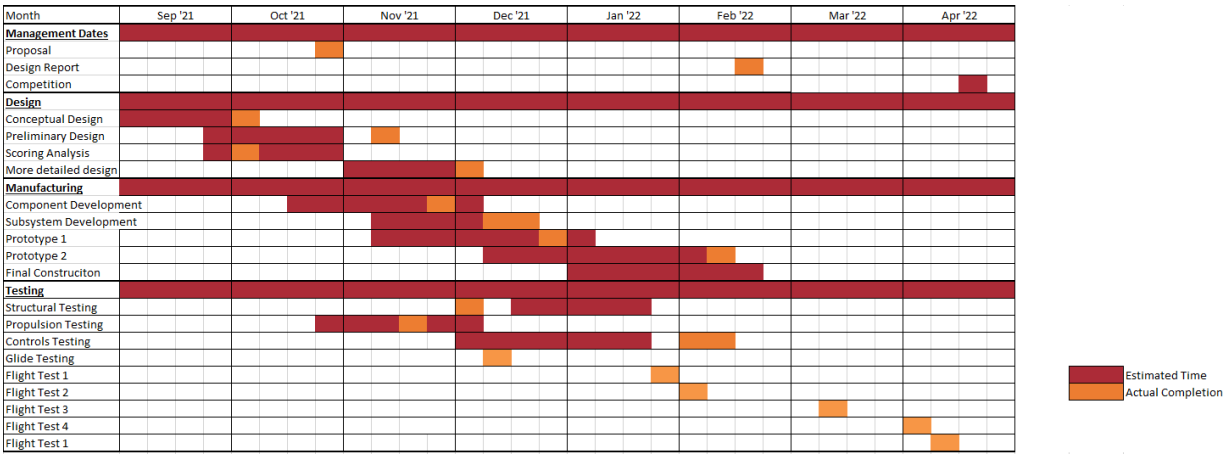

Figure 2: Milestone Chart

Figure 2 is a Gantt Chart which shows the projected major milestone completion dates along with the actual dates of completion. This chart served as a guide to where the team should be in the design and build phases of the project. The chart factored in the due dates of major reports for the AIAA competition, testing and major fabrication deadlines. Throughout the course of this project, this chart was often used to make sure the project was on track to complete everything in a timely manner. In fact, many milestones were hit before the dates projected by the Gant Chart. For example, the team projected the first prototype to be completed in early February, with glide testing occurring between late January and mid-February. The first prototype was completed, and glide tests performed as early as December 15th. The projected dates of completion are in red in the chart and the actual completion dates are in orange for each row.

1.4.2 Team Budget

The team was provided with a total of $1500 from WPI's Aerospace Engineering Department to construct/buy all necessary components for the aircraft. The MQP members utilized the budget to purchase a wide variety of materials and spent a substantial portion of the budget (around 40%) on the batteries and motor for the aircraft. Table 1 provides a rough estimate of the team's budget usage throughout the MQP project. The Aerospace Engineering Department at WPI covered all the costs of travel. The travel budget was around $900 for each team member to cover both plane tickets and lodging.

Table 1: Aircraft Construction Budget Estimation

Type	Summary	Percentage of Total	Cost ($)
Controls Electronics	RC Receivers, Sensors, Servos	10%	150
Propulsion Electronics	Motors, Speed Controllers, Batteries	40%	600
Construction Materials	Carbon Fiber Spars, Balsa Wood, Foam, MonoKote	23.4%	350
Manufacturing Cost	3D Printing, Laser Cutting	5.3%	80
Misc. Components	Landing Gear, Wheels, etc.	6.7%	100
Safety Net	Safety Buffer	14.6%	220
Total	N/a	100%	1500

2 Conceptual Design

The conceptual design of the aircraft began with an in-depth breakdown of mission parameters including flight requirements, rules, and scoring. This process was followed by the scoring sensitivity analysis which allowed the team to prioritize certain design characteristics and develop the aircraft's configuration.

2.1 Competition Breakdown

2.1.1 Technical Requirements

The aircraft design needed to satisfy certain key requirements determined by the competition rules. This included the ability to carry internal payloads, takeoff within 25 feet of runway, and successfully complete a given flight pattern during a dedicated time interval. These constraints helped define the choices for fuselage shape, wing airfoil, and payload deployment mechanisms.

2.1.2 Mission Requirements

The mission requirements presented in AIAA 2021-2022 rules simulate an aircraft capable of transporting humanitarian needs, in particular vaccination components. This portion of the competition comprised of 3 flight missions, each with its own objective, and ground mission. All three missions require the aircraft to takeoff and complete a successful landing. For every mission, the aircraft was not required to land within the allotted time.

2.1.3 Flight Path

Per the competition rules, the take-off field length for the competition was 25 feet for all Flight Missions. Once in the air, the aircraft flew a pre-determined flight path with mission specific number of laps which consist of two 180° turns, a 360° turn, and two 1000 ft straights as depicted in Figure 3.

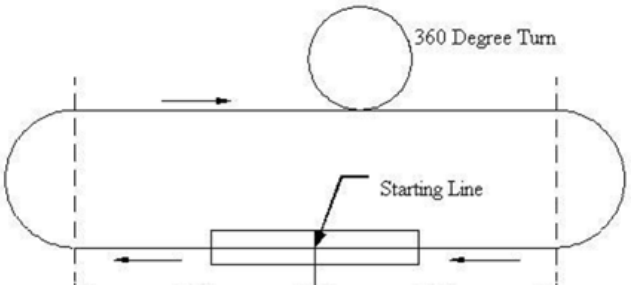

Figure 3: Course Layout, Shown to Scale

2.1.4 Mission 1

Mission 1 tested the basic flight capabilities of the aircraft without any payload. Following a successful takeoff, the aircraft was required to complete three laps of the course within a flight window of 5 minutes. The purpose of this mission was to establish that the aircraft was safe and functional, resulting in either a pass or fail score. Teams who passed were awarded one point while teams who failed were given zero points. Passing this mission depended on a successful takeoff within the takeoff field, a successful landing, and the completion of all three laps. Equation 1 below shows how Mission 1 was scored.

$$M1 = 1.0 \tag{1}$$

2.1.5 Mission 2

Mission 2 was a staging flight where the payload consists of individual syringes with the aircraft required to carry a minimum of 10 syringes. Due to no maximum syringes, the major constraint of this mission was the takeoff weight, and subsequently takeoff distance.

Figure 4: Vaccine Syringes

The syringes being carried in this mission can be seen in Figure 4. Similar to Mission One, the aircraft must complete 3 laps within a flight window of 5 minutes. Scoring of this mission was a function of the number of syringes flown around the course and the flight time. A notable rule in this scoring was that each lap was considered complete once the start/finish line was crossed. This means that the landing after the third lap was not timed, however the aircraft had to land successfully in order to be scored. Equation 2 shows how Mission 2 was scored.

$$M2 = 1 + \frac{N_{\left(\frac{Syringes}{Time}\right)}}{Max_{\left(\frac{Syringes}{Time}\right)}} \quad (2)$$

Where $N_{\left(\frac{Syringes}{Time}\right)}$ & $Max_{\left(\frac{Syringes}{Time}\right)}$ represent the number of syringes/time of the team, and the maximum number/time of all teams in the competition, respectively.

2.1.6 Mission 3

Mission 3 was the vaccine delivery flight where packages were flown through the competition course and deploy on the runway. The packages are 3 x 2.50 x 3.50 inches which can be seen in Figure 5.

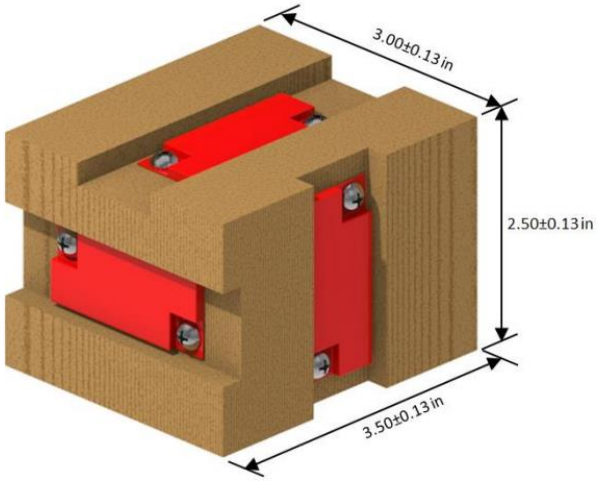

Figure 5: Vaccine Vial Package

Upon arriving at the runway, the aircraft must remotely release the package without setting off any of the three 25g shock sensors. If a shock sensor was activated, it did not count as a successful deployment. The minimum number of vaccine vial packages was one, while the maximum was dependent on the quantity of syringes carried divided by a factor of 10 rounded to the nearest whole number. Scoring for this mission depended on the number of "unbroken" vial packages deployed within the drop area. Equation 3 below describes how Mission 3 was scored.

$$M3 = 2 + \frac{N_{\#successful\ deployments}}{Max_{\#successful\ deployments}} \quad (3)$$

Where $N_{\#successful\ deployments}$ & $Max_{\#successful\ deployments}$ represent the number of successful vaccine deployments of the team, and the maximum number of all teams in the competition, respectively.

2.1.7 Ground Mission

The Ground Mission (GM) was a timed mission conducted to verify the deployment mechanism, and the aircraft's ability to hold all predetermined package/vaccine quantities. The syringes must be loaded and unloaded, in addition to the Mission 3's vaccine vial packages as fast as possible. Equation 4 portrays how the Ground Mission was scored.

$$GM = \frac{Min_{Time}}{N_{Time}} \tag{4}$$

Where N_{Time} & Min_{Time} represents the team's time, and the competition's minimum time to complete the ground mission respectively.

2.1.8 Sensitivity Analysis

Using Equations 1 through 4, as well as educated approximations of what could be designed, and what a maximum score could be, the team analyzed how to prioritize each mission. Using MATLAB, each equation was plotted varying the possible scores and variables to come up with the plot seen below in Figure 6. This analysis helped us to discuss how the team wanted to approach the design of the aircraft to maximize the score.

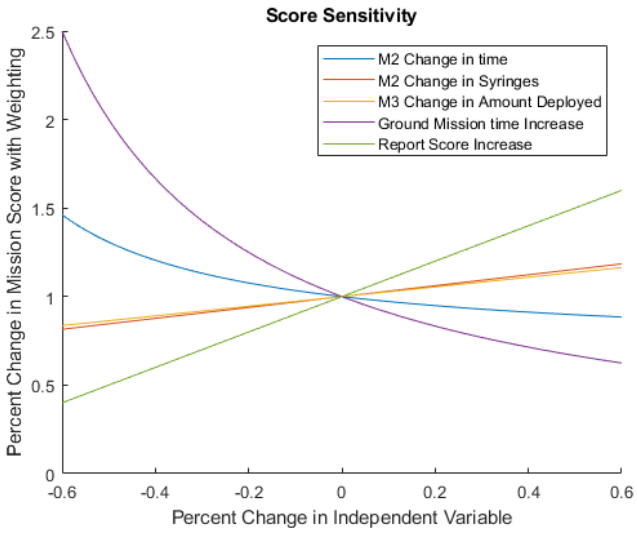

Figure 6: Plot of Score Sensitivity Analysis

Based on this analysis, the time of Mission 2 was extremely important as well as being able to have a great ground mission score. From this analysis and keeping the principal factors in mind the aircraft was designed to hold 40 syringes for Mission 2 and carry 4 packages for Mission 3.

2.2 Subsystem Design Requirements

Following the scoring sensitivity study, subsystem design parameters were determined. The primary subsystems affected by these requirements were the deployment mechanism, fuselage, lifting surfaces, and propulsion systems. The use of these guidelines was critical for the team to be more efficient in design and usage of time.

2.2.1 Payload Deployment

One of the most crucial parts of the aircraft per the sensitivity analysis was the deployment of the vaccine vial packages. This led to a hyperfocus on the effectiveness of the deployment mechanism. It was determined that the mechanism would need to be as simple as possible to reduce the possibility of failure within competition. Additionally, the weight of each deployment mechanism was considered.

2.2.2 Fuselage

Overall, the goal of the fuselage must be to maximize the storage for Mission 2 while not compromising space for the deployment mechanism. Furthermore, this system underwent iterative changes due to other parameters being altered throughout the testing phase of the aircraft development.

2.2.3 Lifting Surfaces

As shown in the sensitivity analysis above a major parameter in calculating the optimal Mission 2 and Mission 3 scores was the change in time per mission. It was important to minimize the takeoff distance to ensure the aircraft can rotate out of the 25-foot takeoff zone while also allowing for a reasonable and controllable cruise velocity. Another parameter to keep in mind was the drag produced by an oversized wing, this would significantly impact the cruise velocity and in adverse conditions could affect the stability of the aircraft. It was ultimately determined that the sizing and airfoil shape would be tested within XFLR-5 simulation software and a wind tunnel to determine the sizing for the wing.

2.2.4 Propulsion System

Within the propulsion system design, there was an overarching goal of maximizing both mission endurance and flight speed. The Mission 3 endurance generates a requirement for ample battery energy as the aircraft would have been in flight for a minimum of ten minutes. Utilizing this requirement, the propulsion system must be optimized for both Mission 2 and Mission 3. This system must also be powerful enough to take-off within 25 feet of throttle up, culminating in the need for a propulsion system that had a high power to weight ratio. Furthermore, the idea of utilizing two different propellers was also considered (2 blade, and 3 blade).

2.3 Configuration and Component Selection

2.3.1 Selection Criteria

Following the analysis of mission scoring, and subsystem requirements, a list of conceptual criteria were created, outlined in Table 2. A Figures of merit system was utilized in evaluating each component.

Table 2: Figures of Merit

Criteria	Score Factor
Aerial Performance	5
Design Simplicity	4
Manufacturability	3
Cost	3
Internal Capacity	3
Structural Strength	2
Controllability	1

2.3.2 Fuselage

When approaching the design of the fuselage, two forms of the structure were considered: Monocoque, and Semi-monocoque. Both structures utilize external members for support and strength such as exterior alumni on commercial airliners and the MonoKote on RC Aircraft. Although true, semi-monocoque uses additional support members such as stringers, and ribs to support the structure. Due to the nature of the design requirements and the need to withstand various loads, a semi-monocoque design was selected.

After selecting the semi-monocoque structure for the aircraft, the shape of the fuselage was determined. Two shapes were seriously considered for the aircraft: Circular, and Rectangular. To determine the design utilized, the team determined figures of merit to compare them which is shown in Table 3. The rectangular fuselage outperforms the circular design as it is far easier to design and manufacture. This is contingent on the use of a semi-monocoque structure in addition to the need for modular ability. This factor, the modular ability, was crucial for the MQP team as alterations to the design throughout the design iteration process were foreseeable. Furthermore, the rectangular fuselage concept provided more storage space for all key components. This was an incredibly key factor as the aircraft's main priority was its ability to carry mission payloads. The only place the rectangular design is weak is within structural strength. Although true, the team reviewed previous MQP reports where this factor was tested. The previous team found that there was negligible difference between the two on drop and compression tests. That team also found that there was negligible difference on aerodynamic effects.

Table 3: Main Fuselage Shape

Criteria	Score Factor	Rectangular	Circular
Design Simplicity	4	2	1
Manufacturability	3	3	2
Internal Capacity	3	3	2
Structural Strength	2	1	3
Total Score		28	22

Based off the FOM (Figures of Merit) table, and the reasoning above, the team decided that the aircraft would be a semi-monocoque structure with spars running the length of the fuselage with rectangular bulkheads perpendicular to the spars. These pieces provide the strength of the fuselage in compression and torsion.

2.3.3 Wing

When addressing the location of the wing on the aircraft, three configurations were considered: Low Wing, Mid Wing, and High Wing. The scoring matrix with the figures of merit utilized is located below in Table 4.

Table 4: Wing Mounting Location

Criteria	Score Factor	Low Wing	Mid Wing	High Wing
Aerial Performance	5	3	3	2
Design Simplicity	4	2	1	3
Manufacturability	2	2	2	3
Internal Capacity	3	2	1	3
Natural Stability	3	2	1	3
Total Score		39	29	46

The team ultimately chose to go with a high wing configuration mounted on a square fuselage. The high volume for payload allowed us to have maximum space for vaccine vials and syringes while also providing relatively high stability and minimal drag.

Another consideration for the wing was the option of wing shape. For these three configurations were given consideration: Rectangular, Circular, and Flying Wing. All these options provided a benefit to the aircraft which is outlined in Table 5 below.

Table 5: Wing Shape

Criteria	Score Factor	Rectangular	Circular	Flying Wing
Aerial Performance	5	2	2	3
Design Simplicity	4	3	3	1
Manufacturability	3	3	2	2
Internal Capacity	3	3	2	1
Maneuverability	1	3	2	1
Total Score		43	36	29

Utilizing these figures of merit, the team decided to move forward with the rectangular wing shape as it outperforms the other wing shapes in nearly every category. The flying wing outperformed the rectangular shape with aerial performance, while underperforming in other metrics which rendered the option unviable. Ultimately, the rectangular shape proved to be the best for the aircraft design.

2.3.4 Motor Configuration

Different motor configurations were considered for the aircraft and have been used by other teams in the AIAA competition. These options include pusher, puller, combination of pusher and puller as well as a two-motor configuration. Most commercial propeller planes use the puller configuration. This is because the propeller gets very clean air with minimal turbulence so more air can be accelerated from the propeller [1]. Pusher configuration, where the motor is on the rear of the aircraft had a benefit of removing electronics and weight from the front but must deal with dirty air, or turbulent air from the fuselage, wing and tail. The benefit of two motor configurations is higher thrust can be achieved however it comes with the drawback of additional weight of itself as well. The two-motor configuration can be used for additional control as being able to operate each motor independently can cause a moment on the aircraft. Another drawback of a two-motor configuration is the limit on battery. Using two motors can easily lead to increased amperage draw from the batteries and can lower overall flight time. Two motor configurations are very good for controllability and thrust but require more battery storage and add additional weight.

To pick the best configuration for the propulsion of the aircraft the team created a decision matrix with multiple options. The three best configurations chosen to consider were a twin propeller design, a pusher motor, and a puller motor, as shown in Table 6. The twin propeller design would consist of two motors that would be mounted on each wing. [8]

Table 6: Motor Configuration

Criteria	Score Factor	Twin Propeller	Pusher	Puller
Aerial Performance	5	3	2	3
Design Simplicity	4	1	2	2
Manufacturability	3	2	3	3
Cost	3	1	2	2
Total Score		28	33	38

Utilizing the decision matrix proved the puller configuration as the optimal motor option for an aircraft with the design parameters. It is noted that it only outperformed the pusher option in the aerial performance figure of merit due to the wake turbulence produced from the wing, hindering the efficiency of the motor.

Another decision matrix was made to find the best type of electric motor to use, an inrunner or outrunner. Two types of electric motor can be used on micro aircraft, inrunner motors and outrunner motors. An inrunner motor had the rotor inside a housing with an output shaft extending through the housing while an outrunner motor had the rotor outside the housing and the whole motor rotates [6]. Inrunners tend to have high revolutions per minute (RPM) with low torque while outrunners tend to have a lower RPM with a higher torque. For an aircraft to have high efficiency while maintaining a lot of thrust, the propeller wants to move a large amount of air with a smaller change in velocity of the air. This can be seen from Equation 5 for thrust below and comparing it to Equation 6 for efficiency. As see from these equations that by increasing the velocity exit of the propeller to gain thrust but lose efficiency. To keep a high efficiency, it is necessary to have a low change in velocities however this keeps thrust low. To raise the thrust and keep efficiency the same it is required to increase mass flow or the area of the propeller. This means that a lower RPM with higher torque is going to be far more beneficial as a larger propeller can be used and therefore, have a more efficient aircraft. With higher rpm, there was a larger variation in velocities. With these facts in mind, the team compared the two types based on efficiency, thrust output cost and complexity to use. The results of this comparison can be seen below in Table 7.

$$Thrust = \frac{1}{2}\rho A(V_e^2 - V_0^2) \tag{5}$$

$$\eta_{Propulsive} = \frac{\dot{m}\, V_0(V_e - V_0)}{\frac{\dot{m}}{2}(V_e^2 - V_0^2)} \tag{6}$$

Table 7: Type of Motor Selection

Criteria	Score Factor	Inrunner	Outrunner
Efficiency	5	4	5
Thrust	3	5	4
Cost	1	3	3
Complexity	1	2	2
Total Score		35	43

The last way you can categorize electric motors is through brushed and brushless. Brushless motors require an electronic controller to change the poles of each magnet to keep the

motor spinning while brushed motors use brushes to physically change the poles [2]. This leads to several advantages of the brushless motor. Brushless motors have longer lifespans as there are no brushes to wear down. They also have higher speed, acceleration, and efficiency. Acceleration was extremely important in this competition as each team was only allowed 25 feet to take off, so a quick take-off was especially important to the aircraft. Because of the clear advantages of the brushless motor the team chose to go with them.

As seen in the scoring of the decision matrices, the best overall configuration for the motor was a brushless, outrunner motor in a puller configuration. This maximized the performance and lead to the best overall propulsive set up.

2.3.5 Battery

Due to competition rules, the battery for aircraft propulsion can be either a lithium polymer (LiPo) or a nickel metal hydride (NiMH). Choosing between each battery type can come with unique benefits and drawbacks based on the chemistry inside that holds the electric charge. LiPo battery packs contain 3.4-volt cells connected in series to increase total voltage of each pack. NiMH battery packs contain 1.2-volt cells and like the LiPo packs are connected in series to form higher voltage packs. A large benefit of using LiPo batteries is that on average they have a higher energy density than most other types of batteries including NiMH. This means the same amount of energy for the airplane can be stored with a lower weight using LiPo batteries. Figure 7 below compares the volumetric and gravimetric energy densities based on bare battery cells. This figure clearly shows the superior energy density of LiPo batteries by weight and geometry than the NiMH counter parts.

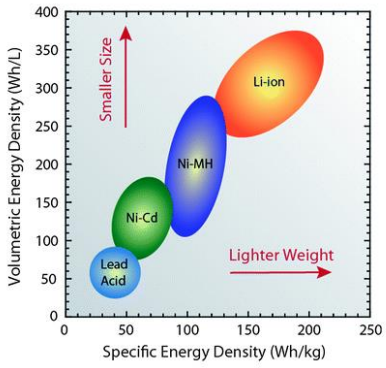

Figure 7: Comparison between different battery cells volumetric and gravimetric energy densities [10]

A decision matrix, seen below in Table 8, was made to compare the different types of battery for the aircraft. The categories that the team ranked these batteries with consist of energy density, overall capacity, safety, and discharge speed. Table 8 depicts these rankings and how they affected battery selection.

Table 8: Battery Chemistry

Criteria	Score Factor	NiMH	LiPo
Energy Density	5	3	5
Overall Capacity	4	5	5
Safety	3	5	2
Discharge speed	2	2	4
Total Score		54	59

Due to the superior energy density, the LiPo battery was the best possible choice for the aircraft. Its low weight as well as the fast discharge speed allowed for a fast take off.

2.3.6 Empennage

When determining the most efficient tail configuration, the aerial performance, design simplicity, structural strength, and maneuverability were considered as the primary figures of merit. This produced three options for the tail configuration: Conventional, T-tail, and V-Tail. A breakdown of these figures can be seen in Table 9. Illustrations of the different options considered can be seen in Figure 8.

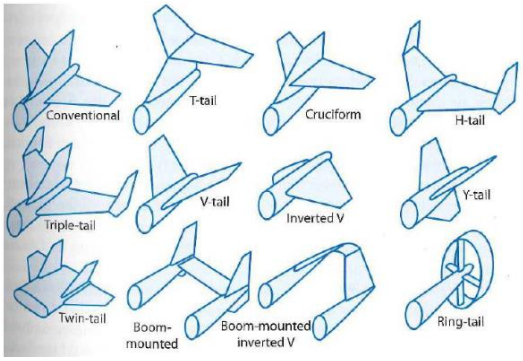

Figure 8: Tail Design Configurations [1]

Table 9: Tail Configuration

Criteria	Score Factor	Conventional	T-tail	V-Tail
Aerial Performance	5	2	3	2
Design Simplicity	4	3	2	1
Structural Strength	2	3	2	2
Maneuverability	1	2	2	2
Total Score		30	29	20

Through this scoring matrix, the team sought to use a conventional tail as the design outperformed the V-tail configuration significantly, and slightly outperforming the T-tail. The aerial performance lost compared to the T-tail is negligible, but the easier design, and structural strength was key when determining the conceptual aircraft.

2.3.7 Landing Gear Configuration

The landing gear selection options were determined by the structural strength, aerial performance, and design simplicity. The configurations considered which should promise for these figures of merit were a tail dragger, and tricycle. The pros and cons of each configuration is shown in Table 10 below.

Table 10: Landing Gear Configurations

Criteria	Score Factor	Tail Dragger	Tricycle
Aerial Performance	4	3	1
Design Simplicity	3	2	2
Structural Strength	2	2	2
Total Score		22	14

Ultimately, the tail dragger option was the most ideal for the aircraft. This was in part due to the aerial performance of the tail dragger, as this added additional angle of attack generated on takeoff. Furthermore, the structural strength was crucial as different portions of the aircraft would undergo stress during the landing sequence.

2.3.8 Payload Mechanism

When approaching the payload deployment portion of the conceptual design, many important parameters were considered. Those being design simplicity, manufacturability, and internal capacity. With these concepts in mind, three unique methods were developed. The first system relied on springs forcing the package out of the aircraft when a servo was actuated. The second utilized two servos both connected to "payload" doors which would then open. The last system utilized doors on hinges that would drop when a half-moon crescent would rotate allowing the door to "drop," releasing the package. All three of these devices can be seen in Figure 9.

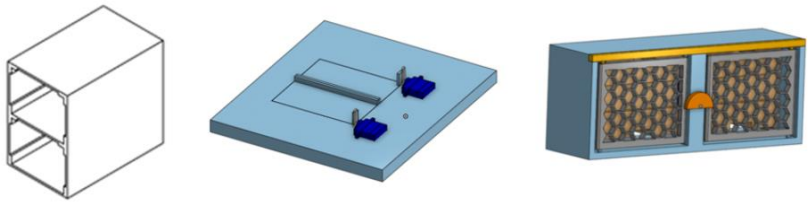

Figure 9: Three Preliminary Deployment Mechanisms

A comparison of these devices can be seen in Table 11.

Table 11: Deployment Mechanism

Criteria	Score Factor	System 1	System 2	System 3
Design Simplicity	4	3	2	3
Manufacturability	3	2	1	3
Internal Capacity	3	1	3	3
Total Score		21	20	30

When looking at the scoring matrix, one can almost instantly see the system utilizing the hinges won as it was the best all-around candidate. System 1 lacked internal space for syringes and would also take a large portion of the internal capacity of the fuselage. Furthermore, System 3 outperformed System 2 when it came to manufacturability as it would be far easier to integrate the system into the aircraft.

3 Preliminary Design

3.1 Design Methodology

After completing the conceptual design of the aircraft, the team divided into sub-teams corresponding to major aircraft systems and areas of interest/expertise as described in the Management section of this report. he individual components of the aircraft were optimized on the sub-system team level until an initial configuration of the aircraft could achieve all mission requirements. This phase concluded with an initial test flight evaluating the design. Once the aircraft completed the test fight, the team would then begin the iterative process of updating and mending the aircraft to be more effective at the mission requirements. The method used for designing and updating the aircraft is showcased below in Figure 10.

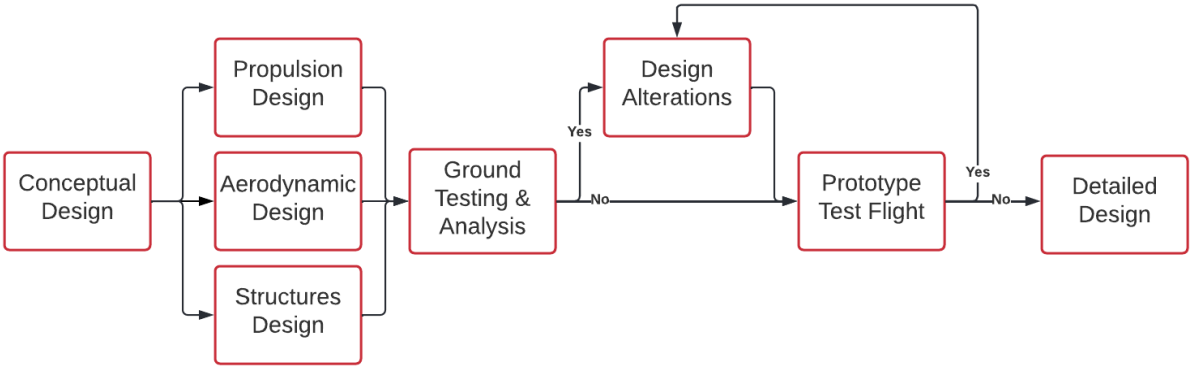

Figure 10: Preliminary Iterative Design Methodology

3.2 Propulsion

3.2.1 Battery

The limiting factor for propulsion generation for the aircraft was based on total stored energy. Due to competition rules, the maximum energy stored for propulsion is 100 watt-hours. The team decided to use LiPo batteries due to the high discharge rates that was needed for the aircraft motors as well as the high gravimetric energy density. Being able to get the most performance out of the motors is mandatory to carry a large amount of payload to complete Mission 3 of the competition. Having high energy density is also especially important since

weight was not shed during flight. Having the lowest weight with the maximum energy capacity was ideal for competition.

Once the use of LiPo batteries was decided on, battery charts were created to understand the capability that each battery would be able to output. The most important thing to measure is total useful Power output and endurance time. Since the rules limit each team to 100 watt-hours of power and LiPo batteries should not be discharged past 85% capacity, the project was left with a useful output of 85 watt-hour. This is total stored energy that flight was limited to for each mission. Once the total energy was known, the maximum endurance power was calculated over the time periods of each mission.

Three batteries were chosen to analyze more deeply. These three batteries were chosen based on total capacity, cell number, maximum discharge rate and total weight of the battery. The three batteries that were chosen are the HRB Graphene 4S 6500 mAh, HRB Graphene 5S 5000 mAh and the DXF 4S 6500 mAh. The specification for each of the batteries can be found in Table 12 below.

Table 12: Battery Specifications

Battery Name	HRB Graphene 4S 6500 mAh	HRB Graphene 5S 5000 mAh	DXF 4S 6500 mAh
Useful Capacity	81 Wh	78.5 Wh	81 Wh
Weight	20.45 oz	23.5 oz	17.28 oz
Voltage	14.8 V	18.5 V	14.8 V
Cells in Series	4	5	4
Max Discharge	422.5 A / 6253 W	500 A / 9250 W	650 A / 9,620 W
Mission 2 Endurance	5 min	5 min	5 min
Mission 2 Endurance Power	972 Watts (66 A)	942 Watts (51 A)	972 Watts (66 A)
Mission 3 Endurance	8 min	8 min	8 min
Mission 3 Endurance Power	608 Watts (41 A)	590 Watts (31.8 A)	608 Watts (41 A)

Using these charts and specifications of each battery, the choices were narrowed down to one. The first important comparison made was between useful capacity, because of the standard milliamp hour ratings of lithium polymer batteries the 4 cell or 14.8 V battery had a higher useful capacity of 81-watt hours which is higher than the 5 celled or 18.5 V battery. This eliminated the 5-cell battery from the selection. Since the team would not be approaching the maximum

discharge rate of either two batteries the next comparison made was the total battery weight. Keeping the design as light as possible with maximum energy density is extremely important to carrying the maximum payload. The DXF brand battery had a lower weight of 17.28 oz compared to the 20.45 oz of the HRB battery. This, along with being able to choose the connector type, was why the DXF battery was chosen.

3.2.2 Motor

Once the battery was selected the next step in designing the propulsion system was choosing a motor. Two types of electric motor can be used on remote control planes, inrunner motors and outrunner motors. As discussed, the team chose to use an outrunner motor due to the high torque as well as the high efficiency. Another important decision the team made was to decide between brushless or brushed motors. The team chose to use brushless motors for many reasons as discussed in the previous section of higher power output as well as higher efficiency.

Once the type of motor was decided on, finding one capable of outputting the correct amount of power was necessary. The first filter for finding rough amounts of power was about 50-100 Watts per pound of the aircraft. This comes from many sources online from the remote-control plane community as well as historical data from previous projects at WPI and professor guidance. For an estimated 12-pound plane this means a power between 600-1200 Watts. The maximum endurance values from the battery data were also used to choose the proper wattage of the motor. For Mission 2 with a minimum endurance time of 3 minutes the battery would be capable of sustaining an output of 1500 Watts. The maximum endurance of Mission 3 would be 8 minutes assuming 2 minutes of payload drop time, resulting in a sustained output of 608 Watts. These values are similar to the suggested power ranges which confirm that a 12-pound aircraft was the maximum weight the aircraft can be to fly with this sized battery.

Brushless motors come with a Kv rating which can be used to describe the power output of a motor. The Kv rating describes the relationship between input volts and output revolutions per minute [4]. This means that for every volt applied the total revolutions per minute can be approximated by the Kv rating times the volts applied.

Three motors were picked based on the criteria outlined in Section 3.2.2 of the preliminary design, this motor needed to be a brushless, outrunner capable of capable of an input power of at least 600 watts. Motors were picked from some of the leading brands in the remote-

control plane industry. The team also investigated what type of motor previous competition winners have been using. The three best motors that were found were the Scorpion SII 3026, Scorpion SII 4020 and the Admiral GP10 5030. These three motors and their specifications are compared in Table 13 below.

Table 13: Comparison of Three Initial Motor Selections

	Scorpion SII-3026	Scorpion SII – 4020	Admiral GP10 5030-400Kv
kV	710	630	400
Max Constant Power	1000 W	1500	1180
Max Constant Current	60 A	95 A	60 A
Weight	7 oz	10.2 oz	13.98 oz
T/W 1100 Watts	(1025) 0.67	(1072) 0.83	No Data
T/W 600 Watts	(600) 0.4	(664) 0.52	No Data

All three of the motors selected have a maximum constant power of at least 1000 watts which is much higher than the 600 watts necessary for Mission 3. However, the Scorpion SII 4020 had the highest constant power of 1500 which is just high enough for a full 3-minute max endurance flight. This is much higher than the next highest of 1180 watts from the Admiral GP10. This means that the Scorpion SII 4020 would be capable of more power for a smaller flight which can help us score better on Mission 2 as it is a time-based mission. The next crucial factor to look at for these motors is weight. The Admiral GP10 which had the middle in terms of power is the highest weight by over 3 oz. Where the two Scorpion motors have lower weights with the 3026 being significantly lower than the 4020. A decision was made to go with the Scorpion 4020 as it had the best power to weight ratio than the 3026 at both 1100 and 600 watts which are the powers that were estimated to be flying at for Mission 2 and 3. This extra weight made up for in its increased power output and capability to run at a higher constant power than the Scorpion 3026.

Choosing a propeller for the aircraft depends greatly on the motor the aircraft was using, and the required thrust and endurance time of the missions. For Mission 2, a shorter mission, can use more constant current than the longer Mission 3. The larger the propeller, the more power it would take to spin. This means that Mission 1 and 2 can use a propeller that is going to be

stronger than Mission 3. The first point of reference is from the manufacturer of the motor. The plane employed the Scorpion 4020 630kv.

Scorpion provides a full data sheet of 25 different propellers and how much current was produced, the revolutions per minute, pitch speed, thrust and effective thrust per watt. This was calculated for 4, 5 and 6 cell LiPo batteries. Using this data sheet, the endurance current of each mission from section 4.1.1 of 66 Amps for Mission 1 and 2 and 41 Amps for Mission 3. Using these current values in the chart and maximizing thrust, the team elected to use the 15x4 propeller for Mission 3 and 15x7x3.

The 15x4 propeller for Mission 3 at 14.8 Volts, the nominal voltage of a 4 cell LiPo battery, based on the data sheet drew 42.5 Amps and produce a static thrust of 124.16 ounces or 7.76 pounds. For a 12-pound aircraft this exceeds the minimum thrust-to-weight ratio of 0.5. The 15x7x3 propeller which was selected for Mission 1 and 2 at 14.8 Volts based on the data sheet drew 75.7 Amps and produced a static thrust of 171.15 ounces or 10.7 pounds. This is well over the 0.5 minimum thrust-to-weight that was designed for the aircraft at 12 pounds.

Each propeller is labeled with two or three numbers which describe the size, pitch and blades of the propeller. The first number is called the arc diameter, or the sized from tip to tip it creates when spinning. The second number is the pitch of the propeller. The pitch is how far the propeller moved through the air for a single revolution. Having a larger pitch meant the plane moved through the air more at the same rpm of a lower pitch propeller. However, it takes more energy to spin a larger pitch propeller. If a third number is present in the name of the propeller it indicates the number of blades the propeller has. If no third number is present it can be assumed that the propeller has two blades.

3.3 Fuselage

After deciding upon a rectangular fuselage within the conceptual design portion of the aircraft development, the structures team focused on the integration of the payload deployment mechanism, avionics, landing gear, wing attachment points, and engine connection. This need formed a complex systems architecture that led the team to implement a modular design which resulted in easy changes between prototype iterations. This proved highly beneficial in the development, and eventual success of the aircraft.

3.3.1 Fuselage Basics

After extensive research into previous AIAA DBF reports, and WPI's Major Qualifying Projects, the team decided to approach the fuselage design utilizing spars, and bulkheads. In the aircraft, 4 spars were used running the length of the aircraft providing extreme rigidity in compression. This was complimented using bulkheads which are extremely rigid in torsion, producing an extremely strong, and rigid base for the aircraft. An early iteration of this design method can be seen in Figure 11.

Figure 11: Early Bulkhead Design

This iteration proved to be extremely strong after drop testing. During this portion of the build, the fuselage was dropped from various heights within the span of 1-3 meters to test the durability of the landing gear and the payload bay / bulkheads. Ultimately due to the success of these tests, this design was utilized throughout the following design iterations, and the final product of the aircraft.

3.3.2 Payload Mechanism

One of the largest challenges of the entire competition is the deployment of the vaccine vial packages in Mission 3. Due to this challenge, the fuselage was built around the payload deployment mechanism. The team's first prototype aircraft contained a dropping mechanism utilizing "Payload Doors" which would swing open when a half moon crescent shape would rotate due to a servo actuation. After constructing this component, system 3 in the conceptual

design, the team attempted to drop a simulated vaccine vial package with the 25g sensors. The design utilizing a payload bay door and hinge can be seen in Figure 12 below.

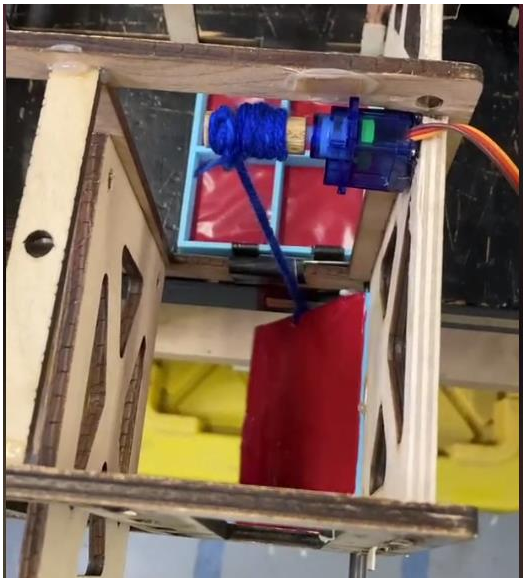

Figure 12: Early Payload Mechanism

During the testing of this deployment mechanism, it was noticed that the shock sensors were tripping, rendering the current payload mechanism useless. This resulted in a complete design overhaul as competition success was based on this system. The new redesigned system lowered the payload down via an "elevator," and then used gravity to tip the box over when a few inches above the ground. The hinge was removed and replaced with yarn run from the winch spool attached to the servo to both sides of the door, allowing the entire door to be raised and lowered as well as rotate. Once the payload was clear of the fuselage bulkheads, the center of gravity being above the mounting points for the yarn caused it to tip over, reducing the fall distance by approximately three inches.

3.3.3 Core Structure

Once the design of the payload deployment mechanism was finalized, the remainder of the fuselage was designed. One aspect the team focused on was modularity of the fuselage. This factor of modularity was crucial in the manufacturing, and iterative process as it allowed for portions of the aircraft to be removed with ease and then replaced. This was especially useful for

when the team conducted payload deployment testing. The aircraft had already begun flight testing with the current deployment mechanism within the aircraft, due to the modularity of the aircraft the interior payload bay was easily swapped and updated with the new design. This was also crucial for flight testing when a component failed due to crashing, it could easily be replaced by an identical piece. This idea resulted in the construction of box joints pieces within the core structure. This method of tabbing allowed the pieces to easily fit together, and then be epoxied together, generating a very rigid structure. This construction technique, as well as the tabbing of pieces can be seen in Figure 13.

Figure 13: Core Fuselage Tabbing Technique

In addition to housing the payload bays of the aircraft, the core structure also housed the avionics, and battery. This section of the aircraft became the hub of the entire fuselage housing all the electronics including the battery, ESC, receiver, fuses, switches, and other flight critical electronics. Looking at Figure 12, the vertical section in the first bay is where the battery would be stored within flight. Infront of the battery section, are guard rails which support the ECS. In

addition to housing mission critical components of the aircraft, it also acted as the connection between the fuselage and wing. This comprised of two carbon fiber rods running perpendicular to the fuselage generating extremely rigid, and strong connection points for the wing.

3.3.4 Wing Attachment Points

The wing attachment design functioned off the core concept that the strongest forces between the wing and fuselage would be in the vertical and tail facing directions. This required the greatest reinforcement over and behind the carbon wing spars. In addition, the wings needed to be removable, and easily reinstalled. Using these constraints, a design was constructed that utilized a hook shape for the larger wing spar, and a snap-in claw shape for the smaller rear spar, as shown in Figure 14.

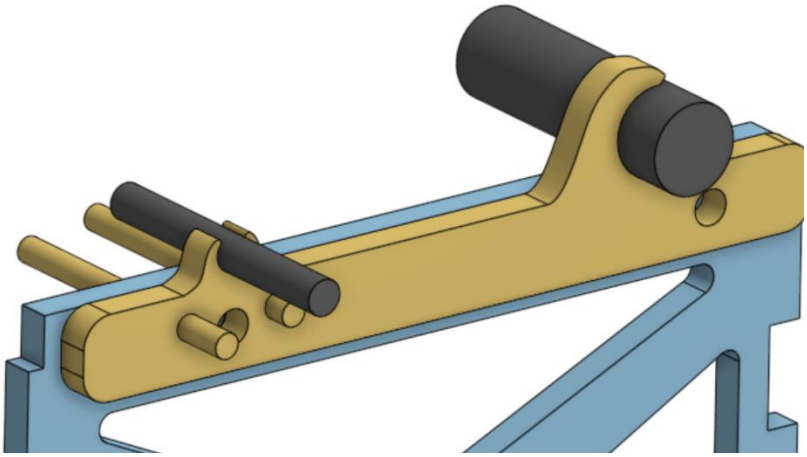

Figure 14: Preliminary Wing Attachment Design

This design allowed the wing to be easily removed by dislodging the rear spar from the claws, tilting the rear of the wing up slightly, and sliding the entire wing forward out of the front hooks. To secure the rear spar in the claw snap, the team utilized thin-gauge aluminum wire in a lashing configuration, which can be seen in Figure 15.

Figure 15: Wing Installation

3.3.5 Landing Gear

The team investigated purchasing premade landing gear from a local hobby store, but none were a proper size for the aircraft. Multiple materials were considered for the landing gear bracket to be made from, including aluminum, steel, and carbon fiber-epoxy. It was decided that the landing gear would be cut out of sheet aluminum with hand saws and then finished with hand files before being bent into its final shape and having wheels attached on a fiberglass axle. When this landing gear proved to be too susceptible to repeated fatigue, the decision was made to use a new bracket made from A36 steel, purchased as a cut flat part from the company SendCutSend, and bent into the proper configuration with a sheet metal bending table. This landing gear, while significantly stronger and able to withstand multiple landings, was much too heavy for the plane to efficiently fly with. This landing gear design was then modified once more. ANSYS structural analysis was used to remove as much material as possible from a gear consisting of 3/8” 6061 aluminum. Once the sheet metal was procured, it was shaped using a Crossfire V1.1 CNC Plasma table to cut the part and a sheet metal bender to complete the shape.

3.4 Aerodynamics

To keep the design of the wing simple, the team decided to use the NACA database of airfoils. Specifically, the team chose to research 4-digit semi-symmetrical airfoils for the main

wing and symmetrical designs for the elevator and rudder. The team chose to use 4-digit airfoils due to their vast documentation and wide use throughout the radio-controlled aircraft.

Historically, radio-controlled aircraft have not particularly needed highly analyzed airfoils to fly well. However, the use of airfoils had only improved the performance of RC planes. When it comes to airfoil selection of small aircraft the predominant factors to look at are speed and generation of lift. The two airfoils the team studied both allow for a high generation of lift while having minimum generation of drag so that the speed of the aircraft is relatively unaffected by the large planform area of the wing.

Using the XFoil Direct Analysis mode in XFLR5, the team analyzed two different historically common NACA airfoils to determine the best choice for the application, the 4412 and 4415. The NACA 4412 results are shown below in Figure 16. The upper left plot is the lift coefficient vs angle of attack in degrees. The peak lift coefficient of 1.4 is quite good as is the 0-angle lift coefficient of 0.5, and the gentle stall as the angle of attack goes between 12 and 18 degrees is desirable for a plane that was doing many takeoffs and landings at slow speeds and higher angles of attack. The upper right plot shows the moment coefficient vs angle of attack. The moment coefficient is negative at all angles of attack, contributing to a stable aircraft. The lower left plot shows the drag coefficient vs angle of attack, with low values around 0.01 at common angles of attack. The plot in the lower right shows the ratio of lift to drag at different angles of attack, showing that the airfoil is quite efficient at lower angles of attack but most efficient around 7 degrees. The NACA 4415 results are shown below in Figure 17. The peak lift coefficient occurs at a similar angle of attack with this airfoil, but it is slightly higher than the 4412 (as is expected with a thicker airfoil) at a value of 1.5. The moment coefficient plot is almost identical to that of the 4412. The drag coefficient vs angle of attack plot shows that this airfoil creates slightly more drag at the low angles of attack. The lift/drag ratio plot shows a higher peak efficiency of 90 at 8 degrees, but a slightly lower efficiency at angles of attack between 0 and 5 degrees.

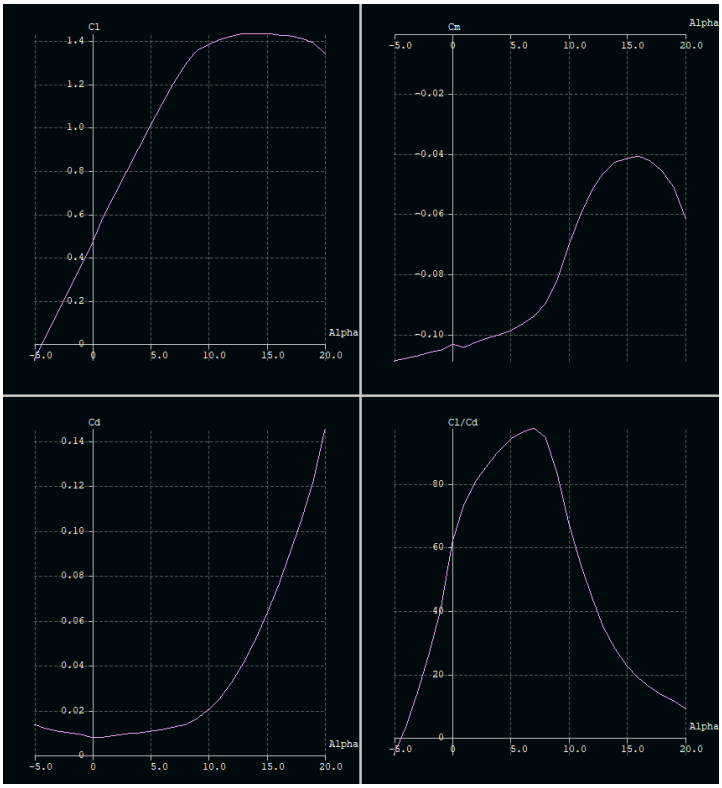

Figure 16: NACA 4412 XFLR5 results

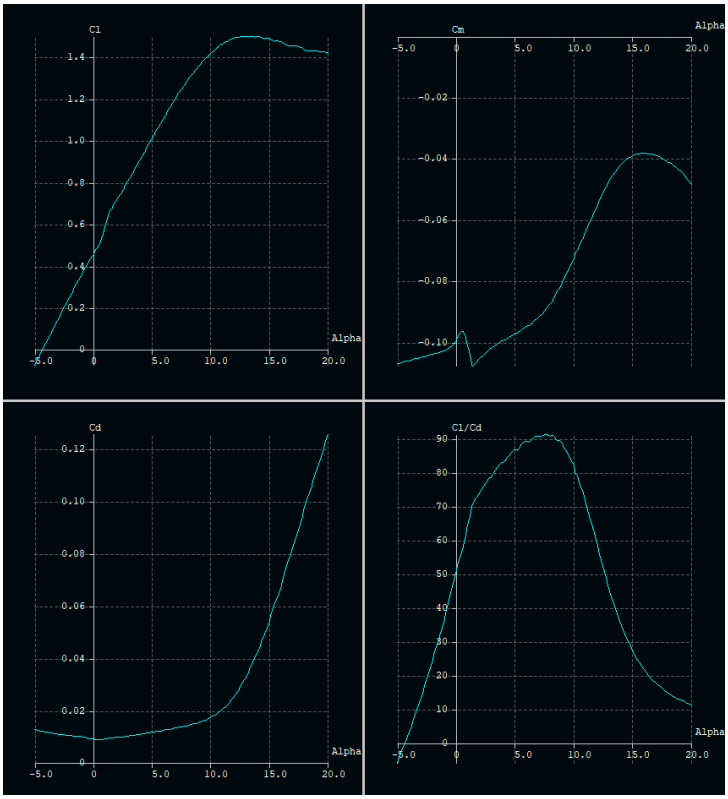

Figure 17: NACA 4415 XFLR5 results

As a result of these analyses, the NACA 4412 airfoil was chosen for the aircraft. It produces slightly less lift but is more efficient in the predicted flight conditions.

The design of the wing was inspired by a modern aircraft wing structure, which utilizes ribs connected by spars to construct the skeletal figure of the wing. On a full-scale aircraft, the ribs are covered in a sturdy metal or fiberglass, but for the application of an RC airplane, Monokote was strong enough to survive the loads produced during the DBF flight. The wing utilized 20 ribs connected to a 0.65" carbon fiber main spar and a 0.25" plastic spar through the airfoil tail. There were six ribs on each side of the wing with the last 2.5" of the airfoil tail to account for control surfaces. Once the team decided how to create the shape of the wing, they determined the size. First, the weight of the plane was estimated be a rough 12lbs by adding all estimated material and payload weights. The AIAA DBF rulebook states that holding the plane at a single point at each wing is similar to applying a 2.5G load.

When sizing the wing the team made an effort to strike a balance between maximizing lift while preserving controllability. It was extremely important to the team that the aircraft was easily controllable and was able to stay stable despite harsh conditions or fast flight speed. It was also chiefly important that the wing was designed with a significant safety factor as the fully loaded weight was estimated to be considerably greater than the empty takeoff weight. This balanced approach allowed the team to focus on important goals and establish the chart shown below when sizing the wing. Table 14 below depicts the goals used by the team to size the wing.

Table 14: Wing sizing goals

Primary Goal 1: Lift Generation	Primary Goal 2: Control Surfaces	Primary Goal 3: Minimize Drag
Generate more than 12 lbs. of lift.	Size wing so that full span control surfaces (ailerons and flaps) can have considerable impact on controllability.	Allow the aircraft to relatively quickly despite all adverse conditions or loading configurations.

Using these values, the determined material properties, and an adequate factor of safety, a structural analysis of the wing was performed using ANSYS. This analysis revealed a maximum deflection of 3.044 cm when two concentrated forces of 60N along the vertical direction are

applied to each wingtip. Figure 18 below displays the result of the structural analysis, where the red coloring indicates the areas of maximum deflection. When compared to the material properties of the main carbon fiber spar and balsa wood ribs, this deflection is acceptable, and the design of the wing was determined to be adequate.

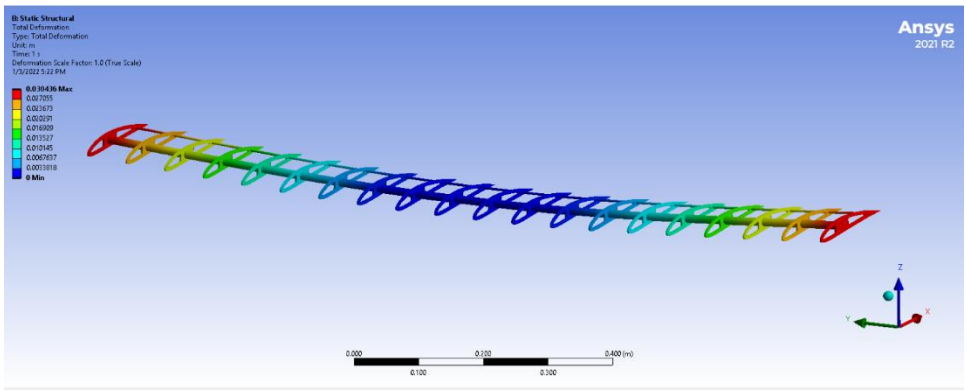

Figure 18: ANSYS Structural Analysis of Wing

To construct the tail, the team cut 2” insulation foam down to a 0.75” thickness and beveled this foam at a 45-degree angle on the top and bottom of the leading edge. This resulted in a very light and effective tail, even without following the distinct curve of a traditional airfoil. In XFLR5, for full scale analysis purposes, the team modeled the tail as a symmetrical NACA 0012 airfoil. To construct the conventional tail shape, they used a plywood spar and glue to create the final shape and plastic hinges to fixture the control surfaces. The servos that controlled the flaps were embedded in the foam for a flush finish. The tail was completed with a MonoKote wrapping to reduce drag.

3.4.1 Controls

From the day of the competition release the team agreed unanimously that one of the most important traits the aircraft should display is high controllability and stability. To take on the problem of controllability the team consulted Raymer [1], which states that an effective control surface must be 33% of the chord length of the wing rib. After sizing the control surfaces accordingly, the next biggest concern was the aircraft's stability when in flight. While cruising it is imperative that the aircraft can be trimmed for optimal and stable flight. Using XFLR-5 the

team was able to analyze the aircraft's ability to be trimmed at various conditions. Figure 19 shows the XFLR5 trim analysis performed.

Figure 19: Trim Analysis of Aircraft During Cruise

When at the established cruise condition with an α of 2° – 3°, the efficiency of the aircraft, represented by the gray line, is only slightly less than maximum. The green dots indicate the efficiency of the aircraft at different trim conditions in the stability analysis. According to the XFLR5 analysis, the tail must be rotated just 0.8 degrees (leading edge down) to obtain this trim with calculated CG.

3.4.2 Predicted Aircraft Performance

The aircraft performed quite well in simulation. For the aircraft to fly well, the team calculated a minimum of 8.5 lbs. of lift was required by the wing for a target empty weight of 8lbs. In simulation the aircraft outperformed this metric with XFLR5 reporting 15.32 lbs. of lift being generated at cruise conditions. Prior to simulation the team estimated a cruise speed of

anywhere between 5 - 9 m/s, simulation reported that the most stable flight of the aircraft would be at 6.923 m/s (22.73 ft/s). Table 15 below shows the estimated performance of the aircraft.

Table 15: Predicted Performance Parameters

Parameter	Mission 1	Mission 2	Mission 3
CLmax	1.42	1.42	1.42
CLcruise	0.68	0.62	0.57
e	0.8	0.8	0.8
CD0	0.08	0.08	0.08
(L/D)max	7.02	6.89	6.78
(L/D)cruise	3.56	3.78	4.21
W/S (lb./ft^2)	1.80	1.98	2.268
Vstall (ft/s)	14.23	14.32	14.01
Vcruise (ft/s)	23.21	22.73	21.32
Gross Weight (lb.)	7.638	8.438	9.638
Flight Time (mins)	5	3 (maximum power)	8 (maximum power)
Takeoff distance (ft)	15 (measured)	18.7 (estimated)	20.5 (estimated)

4 Detail Design

Following the competition of preliminary design and analysis, the detailed design and testing portion began. As mentioned previously, key design traits developed above were incorporated into the finalized aircraft design. Many small-scale improvements were also incorporated into the design of the aircraft.

4.1 Dimensional Parameters

Table 16 shows the dimensional parameters of the final aircraft design.

Table 16: Final Design Parameters

Fuselage Parameters	Length	60 in
	Width	7.3 in
	Height	6 in
	Payload Bay Length	14.6 in
	Taper Ratio	11/12
Wing Parameters	Span	90 in
	Chord	9.5 in
	Area	5.94 ft^2
	Airfoil (NACA)	4412
	Aspect Ratio	9.47
Tail Parameters	Width	22.75 in
	Height	10.75 in
	Horizontal Area	163.54 in^2
	Vertical Area	73.9 in^2
	Horizontal Taper Ratio	0.667
	Vertical Taper Ratio	0.722

4.2 Structural Characteristics

The structural layout of the aircraft, and its subsequent subsystems revolves around the use of carbon fiber spars. Employing this material throughout was crucial when ensuring all loads had an appropriate load-bearing component. Throughout the flight experience and

landings, the aircraft experiences three different forms of loading. The ground loads experienced by the aircraft occur during the take-off and landing sequences. The maximum ground loads the aircraft sustains was when the aircraft was landing during Mission 3, when the aircraft was at its maximum weight. The aerodynamic loads produced include the lift, drag, and moment loads generated on the wing and tail. These loads are transferred through the main wing carbon fiber spar, and the connecting carbon fiber roads in the wing attachment points. The propulsive load is generated by the thrust, and motor torque, which may cause bending, torsion, and vibrations.

4.3 Systems Integration and Architecture

4.3.1 Propulsion

The propulsion system for the aircraft consists of eight main components. These include the motor, two different propellers, an electronic speed controller, a fuse, a switch, battery, and receiver. The motor for the aircraft was the Scorpion SII 4020 630 Kv. The motor would have two optional propellers from Master Air Screw the 15x7x3 and a 15x4. The 15x7x3 is capable of outputting a larger thrust of 10.7 pounds than the 7.76 pounds of the 15x4. However, the 15x7x3 had a much lower endurance time of 3 minutes compared to 8 minutes. The battery used to power the aircraft was a 4 cell DXF battery with 6500 mAh which is under the 100-Watt hour limit of the competition. A 200 Amp fuse was used in an external wiring harness between the battery and the electronic speed controller as safety to protect the battery. The battery is 6500 mAh with a C rating of 100. This means the battery can safely output 650 Amps which is well over the fuse rating. A small on and off switch was wired between the receiver and electronic speed controller as well to have an external switch to turn off the motor. The receiver the team used is the FrSky x8r which is compatible with the FrSky Taranis transmitter already owned by a member of the team. This receiver would allow the pilot to vary the throttle of the aircraft.

4.3.2 Fuselage

The main design characteristic of the fuselage was to hold all mission critical components, including the avionics package, and all mission specific payloads. The fuselage is primarily comprised of multiple carbon fiber spars, and basswood in the form of bulkheads. Structurally speaking, the spars absorb the loads experienced throughout flight and dissipate them throughout the length of the fuselage. The fuselage also serves as the connection point between the tail, wing, and landing gear. The interior of the fuselage was also designed to

accommodate large volumes of payload, including up to 40 syringes, and 4 vaccine vial packages. Figure 20 shows the structure of the fuselage.

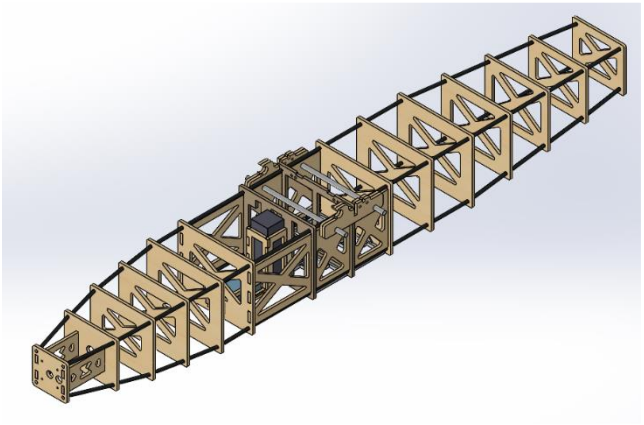

Figure 20: Fuselage Structure

In specifics, four carbon fiber tubes of 0.265-inch diameter are placed at the corners of the bulkheads, and bulkheads of varying sizes are spaced down the spars. Bulkheads are constructed from quarter-inch thick balsa plywood and secured to the spars with hot glue. For the nose assembly, the motor is mounted to a plywood firewall via 4 screws and locking nuts, and the firewall is mounted to two lengthwise struts as well as the carbon spars for strength and stability. The tail mount sub assembly features four simple tabs mounted on the top two spars. The tabs are arranged vertically, and the tail is attached to the tabs with adhesive. For the core structure of the fuselage, balsa bulkheads are attached to balsa sidewalls via a box joint tab method and epoxied to form a rigid structure. This main structure contains the cages for the battery, ESC, and the 4 payload bays. The cages are arranged in the center of the bay, for horizontal stability, and mounted to the bulkheads by box joints. The payload bays feature reinforced sidewalls, and mounts for the door servo motors. The sidewalls also have carbon fiber spars of 0.38-inch diameter running through them parallel to the wing spars. These serve as the mounts for the wing attachment brackets. The brackets are used in tandem on either side of the fuselage, and feature an updated design shown in Figure 21.

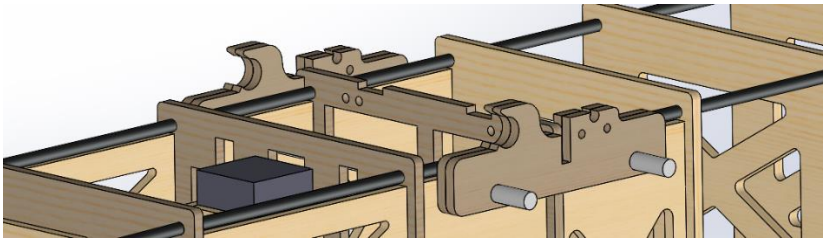

Figure 21: Updated Wing Attachment Bracket

The larger wing spar is slotted at an angle into the front hook on both sides of the fuselage, and then rotated down to snap the rear spar into the back slot. To lock the rear spar in place, an aluminum U-shaped locking bracket is used with a pair of locking cotter pins. The bracket is oriented with the U bend over the rear spar, sandwiching the spar in between the claw of the mounting bracket and the locking bracket. This design, seen in Figure 22, proved to be sufficiently strong as well as easily removable for transporting the aircraft.

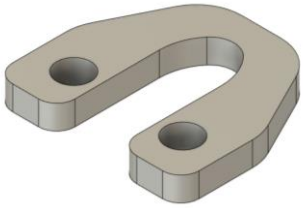

Figure 22: Wing Locking Bracket

The installed wing can be seen in Figure 23, including the mounted spars, and the locking pins.

Figure 23: Wing Mounted to Fuselage

The A36 steel landing gear used in the preliminary designs proved to be overly heavy and weak to continuous loading. Due to the bracket bending outwards during every landing, the decision was made to test new materials and designs. After sufficient FEA testing, a new bracket design was chosen and constructed using a sheet of 6061 aluminum. This bracket was cut using a CNC plasma cutter and bent into shape using a sheet metal bending table. To attach the wheels, each side uses a winged M5 bolt and a pair of locking nuts, as shown in Figure 24. The final design removed 4 ounces of weight compared to the steel bracket and was over 1.5 times as strong.

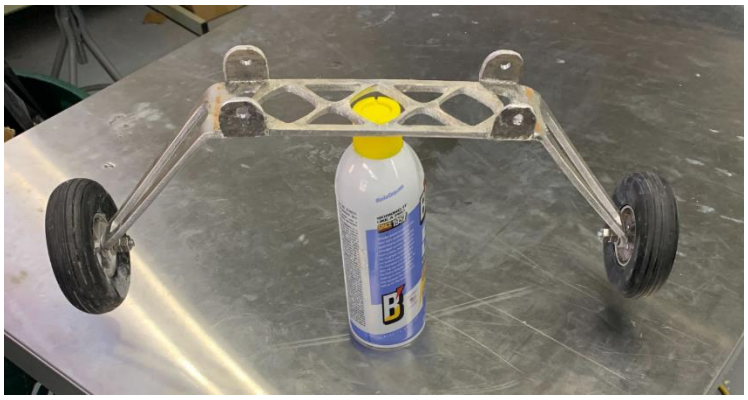

Figure 24: Final Landing Gear Design

4.3.3 Aerodynamics

The aerodynamics systems include the wing and tail components. These systems closely relate to others, such as the controls and structure of the aircraft. The wing was built using a rib and spar configuration of balsa wood and carbon fiber. Each rib is a NACA 4412 airfoil of laser cut wood, with a chord length of 8.5”. There are 20 ribs total: 9 ribs in each side of the wing and 2 ribs as part of the wing attachment to the fuselage. The ribs are connected with carbon fiber spars. The main spar is 0.65” while the secondary spar is 0.25” in diameter. The wing is 72” in total and is finished with MonoKote. The tail was made from XPS insulation foam and were cut into shape with a hot wire foam cutter. The tail had a 1/4” thick plywood structure in an inverted-T shape embedded within it providing strength and stiffness. The control surfaces on both the wing and tail were also created using XPS foam and were connected to pushrods and servos linked to the transmitter. They were attached to the aircraft’s ribs and tail with nylon hinges. The final design of the aerodynamic systems can be found in Figures 25 and 26 below.

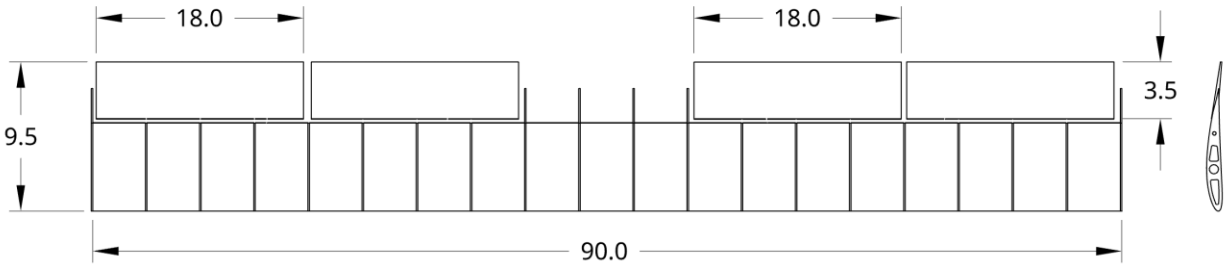

Figure 25: Detail Design of Wing (unit: inch)

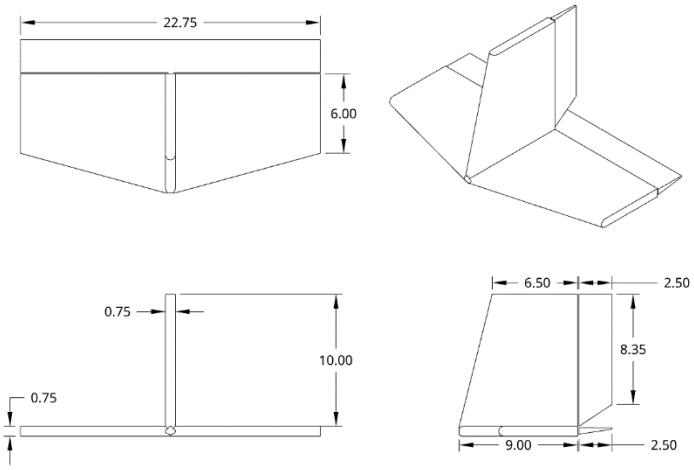

Figure 26: Detail Design of Tail (unit: inch)

4.3.4 Controls

The control system for the aircraft consists of the transmitter on the ground and the components in the aircraft, shown below in Figure 27.

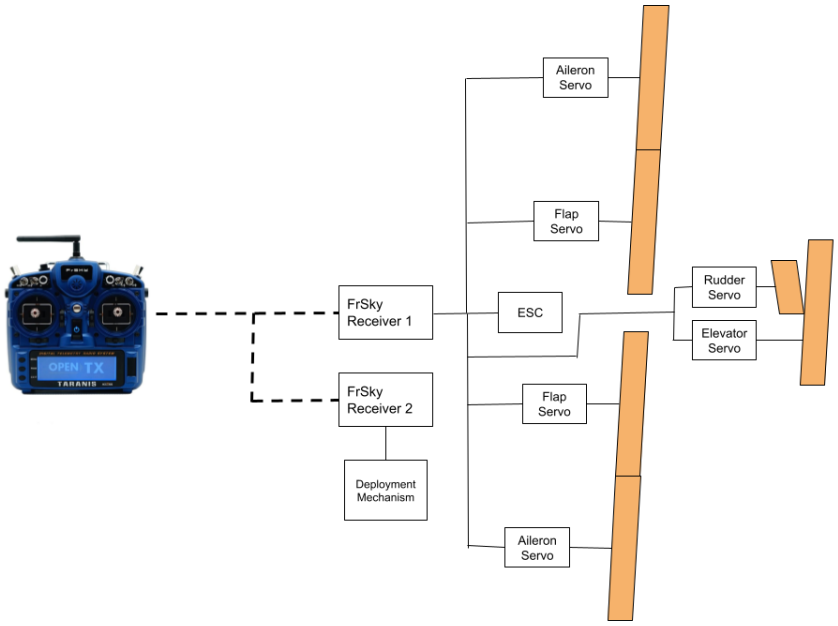

Figure 27: Diagram of Control System

The transmitter is a FrSky Taranis, operated by the pilot to communicate with the two FrSky X8R receivers in the aircraft over 2.4ghz. This transmitter was chosen for its programmability, allowing the team to fine tune flight controls as well as providing plenty of options when it comes to actuating the deployment mechanism. Additionally, the range is estimated to be one mile line of sight, providing a secure connection to the aircraft for all testing and the competition. The first receiver in the aircraft was dedicated to the flight controls and the second is dedicated to the payload deployment mechanism. The receiver channel mapping can be seen below in Table 17.

Table 17: Channel Assignments for Control System

Receiver #	Channel #	Description	Receiver #	Channel #	Description
1	1	Throttle (ESC)	2	9	Deployment Mechanism
	2	L Aileron Servo		10	
	3	R Aileron Servo		11	
	4	Elevator Servo		12	
	5	Rudder Servo		13	
	6	L Flap Servo		14	
	7	R Flap Servo		15	
	8			16	

Each of the six flight servos is connected to its respective control surface by a pushrod and control horn, as shown below in one aileron control surface and the elevator control surface in Figures 28 and 29 respectively. All servos are recessed into the aircraft as to not disturb the airflow over the control surfaces. The aileron, flap, and rudder servos are Hitec HS-425BB servos while the elevator servo is a Futaba S3010. The Hitec servo was chosen for its high torque at a reasonable price, and the Futaba servo was chosen for its even higher torque since it was moving the largest and most critical control surface.

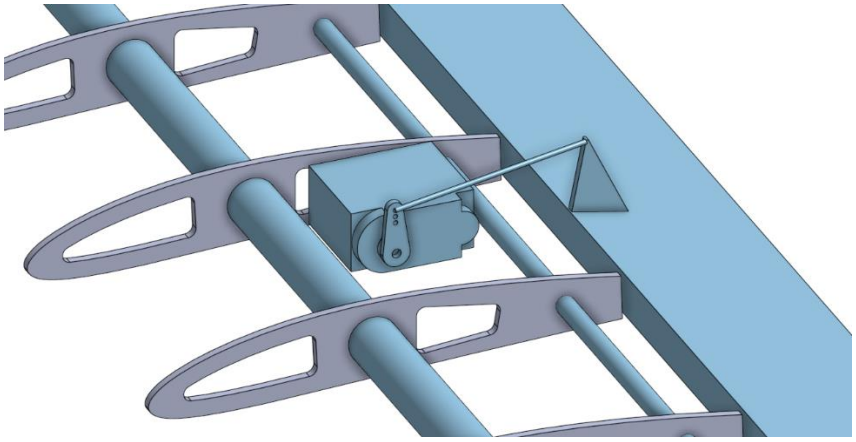

Figure 28: Detail CAD of Aileron Mechanism

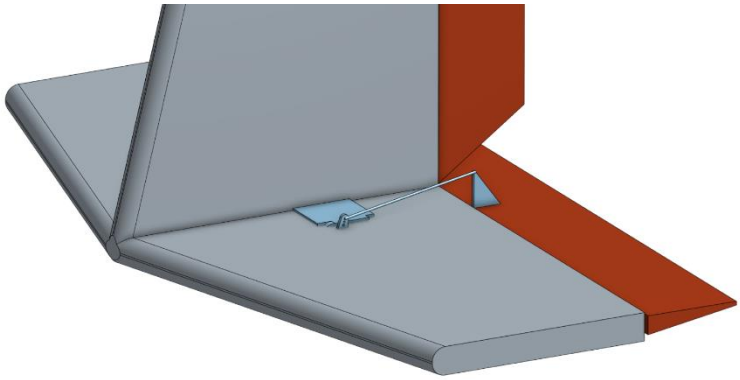

Figure 29: Detail CAD of Elevator Mechanism

4.3.5 Payload Deployment Mechanism

The payload deployment mechanism consists of four identical payload bays, each designed to lower one payload. The servo that acts as a winch for each bay receives power and signal from one channel of the second receiver. Figure 30 below shows the payload mechanism without payload, with red lines drawn to illustrate the path that the fishing line follows to connect the platform to the winch. Dotted lines indicate the line being partially or totally blocked from view by the fuselage. In the third image, the platform is lowered to deployment height.

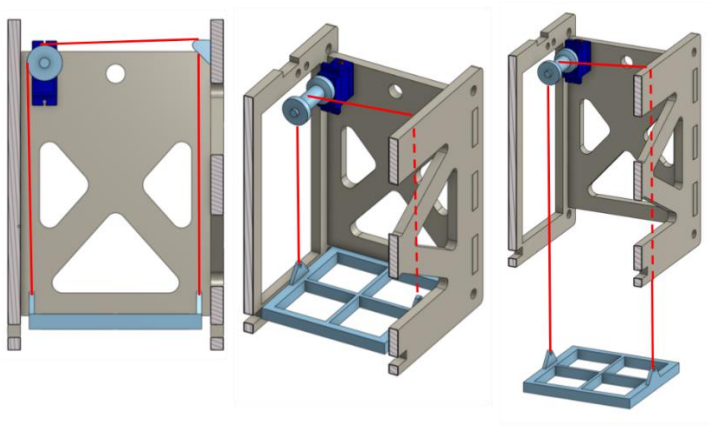

Figure 30: Detail CAD Design of payload deployment mechanism

Figure 31 below shows the payload mechanism going through the three stages of operation. During takeoff and flight, the platform is raised, securely holding the payload within the aircraft.

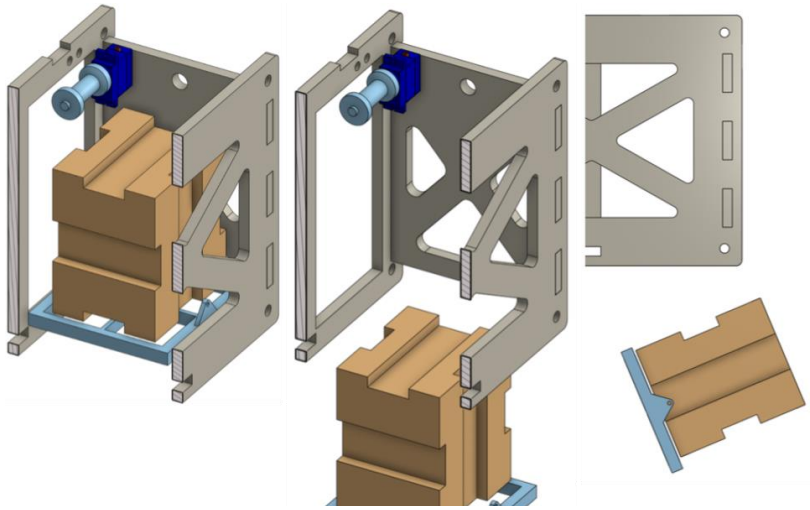

Figure 31: Detail CAD Design of payload deployment mechanism with payload

Once on the ground in the payload deployment area, the servo rotates, lowering the payload down until it exits the aircraft. At that point, the platform and payload tip over, dropping the payload the remaining approximately 2 inches to the ground.

At the competition, further testing and ground mission attempts indicated that the payload was still falling too far as well as landing with a rotational shock, setting off the sensors. To address this, the team worked through multiple iterations and identified a configuration that set the package down extremely gently. Two more strings were added to each payload mechanism: one to force the door to rotate at a specific point and in a specific direction and another to soften the tipping of the payload onto the ground once the door was fully rotated. The detail design of the final version of the payload mechanism can be seen in Figure 32, with the red lines representing the preexisting winch strings, the blue line representing the third string with a fixed length that caused the door to rotate as it descended, and the green lines representing the fourth string that wrapped around the payload and held it in place as it descended and cushioned the rotation as it deployed. The blue string was attached to the upper carbon fiber fuselage spar (not pictured).

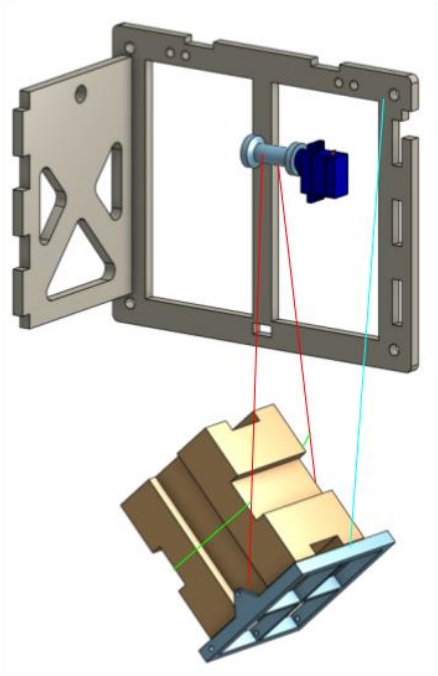

Figure 32: Final Payload Deployment Mechanism

4.4 Overall Aircraft Performance

The final configuration of the aircraft fell within the dimensional limits that the AIAA DBF Competition rules set out. Specifically, the fuselage of the aircraft was 60 in long and the main wing was 90 in wide. Additionally, the tail was 10.75 in tall and 22.75 in wide. The aircraft sat naturally at a slight upwards angle at approximately 5.5° thanks to the configuration of the landing gear. The final fuselage configuration allowed the aircraft to safely carry either 2 vaccine vial package or 20 or more syringes. The fuselage suffered several drops and crashes and showed only signs of minor breakage even during the most intense crash it suffered. The modular design also allowed the team to rapidly prototype new design configurations. With the reduced number of payload bays the weight and balance characteristics of the aircraft have changed significantly. Table 18 below shows the important mass values for each of the three major missions.

Table 18: Mass values for each mission

Mission #	Total Mass (lbs.)	Vaccine Vial Mass (lbs.)	Syringe Payload Mass (lbs.)
1	7.638	N/a	N/a
2	8.438	N/a	0.8
3	9.638	1	N/a

For the flight tests, the team based the success of the test based on a few easy to analyze parameters. The first is takeoff distance, as per the rules of the 2021-2022 DBF Competition all aircraft must takeoff within the 25-foot field, so if the aircraft was able to takeoff before 25 feet then takeoff had been successful. The next parameter, and most important for the team, is controllability at competition altitude. Once the aircraft reached an adequate altitude to complete the flight plan, the pilot tested the aircraft's ability to yaw, pitch and roll in every direction and tested the aircraft’s ability to fly in a straight line after being trimmed properly. The team used the WPI track and football field to measure distances and give the pilot a rough flight plan to follow along the path of the track. If the aircraft could complete the basic maneuvers the pilot inputs and fly around the track, then the test was successful. The final parameter observed was the speed and endurance time of the aircraft. While the team did its fair share of due diligence in calculating the battery draw and depletion time for each mission, hitting the target speed during

the competition was paramount to evaluating whether the aircraft could complete the course in an optimal amount of time.

5 Manufacturing

This plan documents the processes and materials investigated for major component manufacturing. Also included are major manufacturing milestones for system components, and a schedule of those milestones, planned and actual.

5.1 Manufacturing Processes

5.1.1 Balsa Construction

For the components of the aircraft what were manufactured using balsa plywood, the team used a laser cutter to create the parts. There were a few options available to the team regarding wood manufacturing, including hand saws, band saws, and the laser cutter. After weighing the pros and cons of each method, it was apparent that the laser cutter was the most effective process. The laser cutter was much more precise and time efficient than cutting each piece by hand. Worcester Polytechnic Institute offered two laser cutters to the project to get the job done: both Full Spectrum P-Series of dimensions 48x36 and 24x18 in.

5.1.2 3D Printing

In the conceptual phase of the project, the team designed some components that could not be constructed using balsa wood. These components would have to be 3D printed. The team had many FDM printers available to use. Worcester Polytechnic Institute offers the use of Ultimaker 3's and Lulzbot TAZ 6's, which were utilized for the purposes of this project. The team also used some of the member's personal printers, which included Ender 3s and an Ender 5. All these printers were used with PLA. While WPI also offers a Stratasys Dimension 1200 and Objet30 for ABS and resin printing, the team decided that PLA was sufficient for the purposes of this project due to its desirable strength-to-weight ratio and ease of construction.

5.1.3 Foam Construction

In addition to wood and plastic, there were some components that were chosen to be created using 2 in XPS insulation foam. This foam was quite sturdy and easy to work with. It was also incredibly light and strong. The lab utilized for this project had a few different methods of working with this foam. One was a Lenox utility knife, which cut the foam quite well.

Another was a Hercules 8500 DHWT hot wire foam cutter. This worked much better than the utility knife and was the preferred method of working with the insulation foam.

5.1.4 Machining

There were certain components that were required to be quite durable and support multiple times the weight of the aircraft. For these parts, the team considered manufacturing them through machining. WPI's Washburn Shops offer many machines to machine parts from stock, including three Haas ST-10 lathes, a Haas ST-30SSY, three Haas MiniMills, and a Hypertherm Powermax 1000 G3 Series plasma table. Bar stock of an assortment of materials could easily be purchased from McMaster-Carr. The team was trained in the machine shop for most common materials, including aluminum and steel, so the members had adequate access to any tool or machine required to create the correct components of the aircraft.

5.2 Manufacturing Process Selection

5.2.1 Wing Construction

To manufacture the aircraft's wing, the team chose to utilize ribs of the chosen airfoil, connected with spars. As described above, a few different manufacturing processes were available to create the ribs, including 3D printing, laser cutting, and machining. The team first had to consider the material the ribs would be created from, and how different materials correspond to the manufacturing processes offered to the project. Machining was quickly ruled out because of the unnecessary difficulties and complexity that is characteristic of the process, especially when compared to the other manufacturing options. Creating the ribs out of aluminum would also add too much weight to the aircraft and while they would be strong, they would be much stronger than the parts are required to be. 3D printing the spars were ruled out next. While 3D printing is an easier process than machining, the number of ribs required for the aircraft's 6ft wingspan would make for large print times. Printing with a plastic filament, such as PLA, would cut down on the wing's weight, but the team felt there was another option better suited for the project's needs. The team decided to cut the ribs out of balsa wood with a laser cutter. The cuts could be completed in a matter of minutes and balsa wood is extremely light. After ANSYS testing with estimated loads, the wood was fortunately found to be strong enough to support the aircraft during flight. While running the ANSYS simulations, the team also chose the material of the spars to connect the ribs. Both wooden and carbon fiber rods were considered, but carbon

fiber proved to be best for both weight and strength. The ribs can be seen after laser cutting in Figure 33 below.

Figure 33: Laser Cut Wing Ribs

Once the ribs were laser cut and the carbon fiber spars were acquired, the wing was assembled using hot glue as a temporary fixture. The team planned on using epoxy to secure the wing assembly, but the hot glue proved to be much stronger than anticipated and didn't budge during testing, while also being removable and easier to work with. Once all 20 ribs were secured to the spars, the wing was covered in Monokote, and the team got to work on the control surfaces. The wing can be seen before Monokote in Figure 34 and after Monokote in Figure 35.

Figure 34: Wing Ribs Attached to Spar

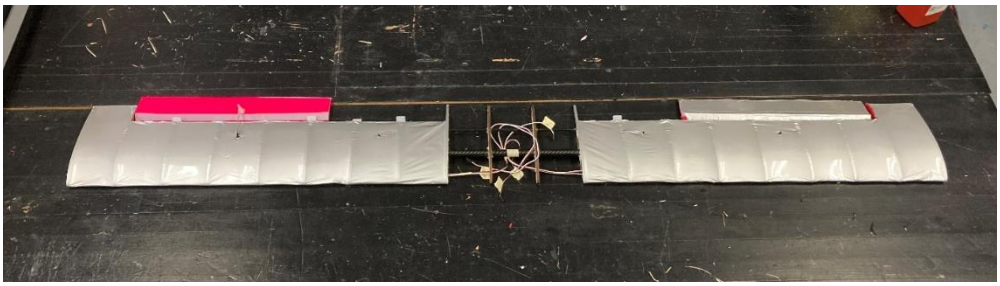

Figure 35: Wing after Monokote (before the flaps were added)

The flaps and ailerons were manufactured out of XPS insulation foam using a hot wire cutter. Once they were cut to shape, they were covered in Monokote and attached to the wing with nylon hobby aircraft hinges. The control surfaces were connected to a push rod, control horn, and then a servo that moved the mechanism. The servos were installed before Monokote and wired to a receiver that was linked to the transmitter.

5.2.2 Fuselage Construction

Figure 36: Core Fuselage Construction Technique

The fuselage of the aircraft was constructed using a combination of wooden bulkheads, and carbon fiber rods, as seen in Figure 36. The carbon fiber rods acted as spars running the entire length of the aircraft's fuselage. Within the aircraft, ¼-inch thick plywood is used as the core material. To have precise measurements and cuts, a laser cutter is used to cut all bulkheads and sidewalls for the fuselage. In the middle of the aircraft was the core structure of the aircraft

which houses the avionics, payload bays, and wing attachment connections. This portion of the aircraft was primarily ¼-inch thick plywood as it undergoes extreme structural stress. Within this section, the pieces are connected using notches, and tabs which allow the core to conjoin, and provide extra strength. These are then epoxied together to form the core structure of the fuselage.

From this point, the carbon fiber rods are placed in the core structure extending out of the core on each side. This is then hot glued into, place. The tail section of the aircraft was constructed next, utilizing the bulkhead method, they are slide on one at a time. The distance between each bulkhead is then measured to match the CAD model then hot glued into place. This method of using bulkheads, and carbon fiber spars can be seen in Figure 37 below.

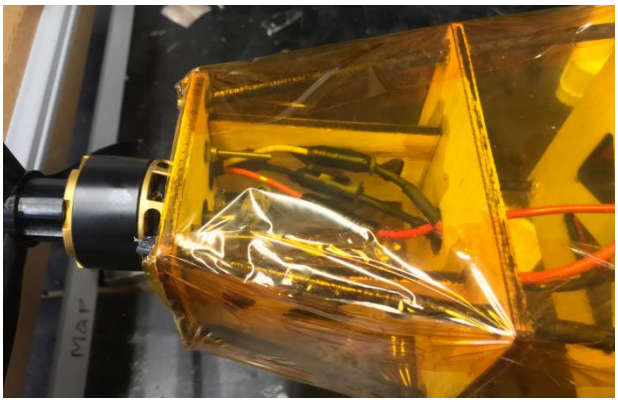

Figure 37: Front Engine Showing Carbon Fiber Spar/Bulkhead Construction Technique

The tail also experienced a taper which resulted in the carbon fibers rods being compressed, adding additional strength. At the front of the aircraft, the landing gear was slid onto the bottom two carbon fiber rods. After placed on, it was hot glued in place to the carbon fiber rods. The remainder of the nose cone was connected via the method the tail was secured with as well.

5.2.3 Landing Gear

The landing gear was required to be strong enough to withstand a heavy landing with mild to no deformation. This means the material had to be stronger than 3D printed plastic or balsa wood, both of which could easily splinter and break under substantial loads. After repeated failures with a thin sheet metal aluminum bracket, the team decided to manufacture the landing gear out of A36 mild steel. the team elected to send a .DWG file of the unbent landing gear to SendCutSend, a metal cutting company. Two copies of the landing gear were cut by waterjet and

shipped by SendCutSend, an online laser and CNC cutting service. Once the landing gear was acquired, the team manually bent it into shape and drilled holes to remove material to decrease weight. Holes were drilled using a half inch drill bit and then connected by cutting with a Dremel and angle grinder to remove the target areas. Finally, the rough edges were filed down using hand files and a sanding wheel on the Dremel. The landing gear can be seen below in Figure 38 in an intermediate stage of manufacturing, and in Figure 39 before the third flight test.

Figure 38: Steel Landing Gear in Progress

Figure 39: Steel Landing Gear Installed on Aircraft

After this bracket proved to be too dense and susceptible to bending during landing, innovative designs were proposed and tested against the steel bracket. The team first planned on using the second unbent steel bracket and the plasma cutter to remove interior material, however FEA testing showed that this design would be insufficient in strength. The final design was produced, tested, and CAM-ed in Fusion360, as shown in Figure 40. The design maintained the overall shape of the previous bracket, however it featured key reductions in weight, and was fully cut using the Washburn Shops CNC plasma table. The plasma table was chosen over another SendCutSend order because it was more cost effective, allowed rapid design alterations and could immediately be tested for fatigue during landing.

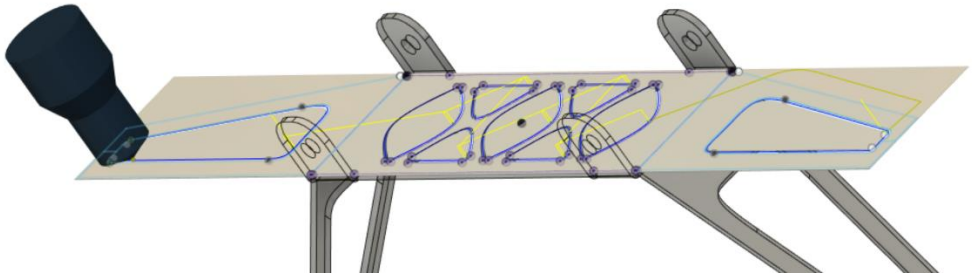

Figure 40: CAM Simulation of CNC Plasma Cutting Table

This bracket was made from a 3/8-inch sheet of 6061 aluminum. This increased the thickness of the bracket and its resistance to bending, but still lowered its overall weight to 6.272 ounces. The plasma table does have dimensional tolerance limitations, and cannot do small, detailed cuts as a waterjet cutter can, but was sufficiently accurate for the construction of the bracket. After cutting, the bracket was post-processed with a grinding wheel and hand files, and the mounting holes were reamed out with a drill press. The flat bracket can be seen in Figure 41.

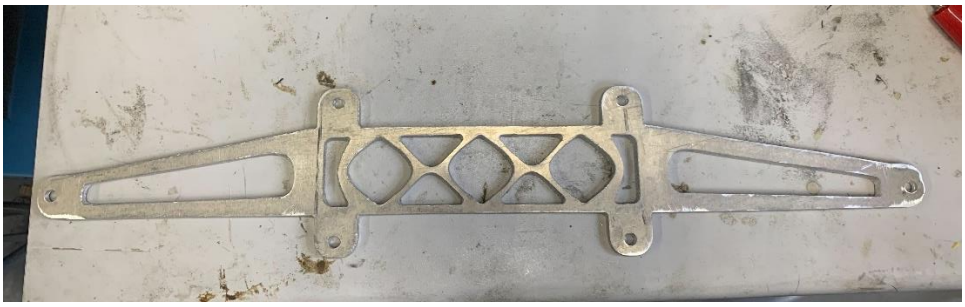

Figure 41: Flat Cut of Aluminum Bracket

To bend the bracket into place, heat was applied from a propane torch while the bracket was bent with a sheet metal bending table. This bracket proved to be the final iteration and was used during flight at the competition.

6 Testing Plan

6.1 Testing Schedule

The team created a comprehensive testing plan that addresses each sub-system and sub-assembly. Table 19 below is a complete list of the types of tests and their respective dates of completion.

Table 19: Testing Schedule

Test Name	Date of Completion
XFLR5 Stability Test	11/15/2021
CFD Testing	11/25/2021
Thrust Stand	12/2/2021
Glide Tests	12/15/2021
Drop Test	12/16/2021
Control Surface Testing	01/24/2022
Flight Test 1	01/26/2022
Flight Test 2	02/02/2022
Payload Drop Test	02/08/2022
Flight Test 3	02/22/2022

6.2 Propulsion Testing

Once all the selected parts arrived, testing began the propulsion system for the aircraft. The six components for the propulsion subsystem are the motor, electronic speed controller, battery, receiver, transmitter, and propeller. The motor chosen was discussed above and was the Scorpion SII-4020 630 kV. The electronic speed controller or ESC used was the Scorpion Tribunes II 120 A. The battery the team used also discussed above was a 4 cell 6500 mAh from DXF Power. The receiver used was a FrSky X8R with a corresponding FrSky Taranis X9D transmitter. The two propellers used were both from Master Airscrew and were the 3 blade 15x7 and the 2 blade 15x4 propeller. These are the main components that drive the propulsion sub assembly.

To test the subsystem, the team used a RCBenchmark 1585 test stand. This thrust stand was capable of measuring thrust, torque and revolutions per minute in conjunction with being able to read the voltage and current of the motor through the ESC the team was able to record data for the aircraft's electrical subsystem. Using this thrust stand, the team was able to put it inside the wind tunnel in the Worcester Polytechnic laboratories to measure thrust at different airspeeds. A picture of the thrust stand for static testing can be seen below in Figure 42.

Figure 42: Thrust Test Stand

This propulsion system worked as intended and all the propulsion parts were compatible. The team was able to control the thrust using the transmitter and the thrust that it generated was extremely similar to what was expected. Data was collected for both static tests and inside the wind tunnel at different airspeeds. Plots were created with all the data and can be found in section 7.1. The propulsive subsystem worked as intended and the testing confirmed this.

To comply with the competition rules as well as ensure that the team was being as safe as possible, the first thing done was wire a switch between the separate 11.1V 1.5Ah LiPo battery and 5V converter that powers the receiver and servos. This switch was mounted externally and be able to turn on and off the radio control system. The other safety measure implemented was an external bullet connector loop that formed a jump between the electronic speed controller and the battery. On the battery side of this connector jumper system, the 200 Amp fuse was

connected as close as possible to the battery. This 200 Amp fuse was less than the maximum output of the battery and would provide the safety for the aircraft and battery system. A diagram of how the system was wired can be seen in the Figure 43 below.

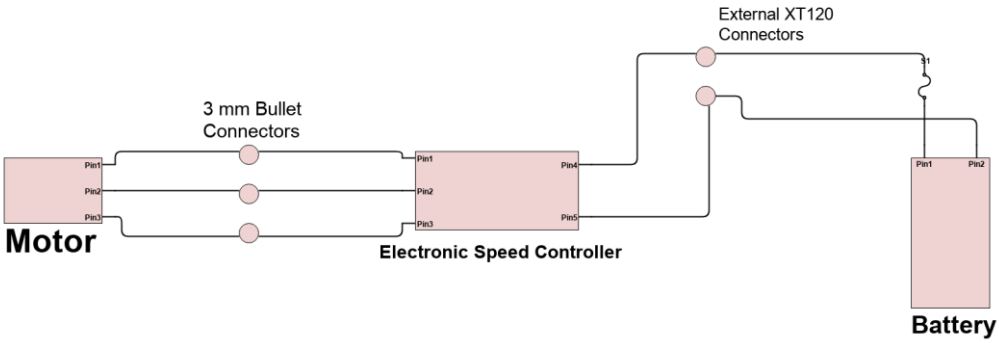

Figure 43: Wiring Diagram for Propulsion System

6.3 Structures Testing

Testing of aircraft structures was done through Finite-Element-Analysis (FEA) on key aircraft subassemblies, and through physical loading tests, such as drop testing, and landing testing.

FEA analysis was performed in the software packages ANSYS Mechanical and Fusion360. Due to the size of the aircraft, the fuselage was broken down into smaller subassemblies and FEA static loading analysis was performed on these subassemblies. These include the nose, tail, payload bay, wing mounting brackets, wing, and landing gear. In a static loading test, certain features in an assembly are fixed, or immovable, and defined loads are applied to other features. The test calculates the strength of the design, the safety factor, and defines a map of the areas under the greatest stress.

This can be seen in Figures 44 and 45, which show the difference in calculated deformation and stress between the steel landing gear design and the final aluminum bracket design. The steel design experiences much greater deformation and stress in comparison to the aluminum design.

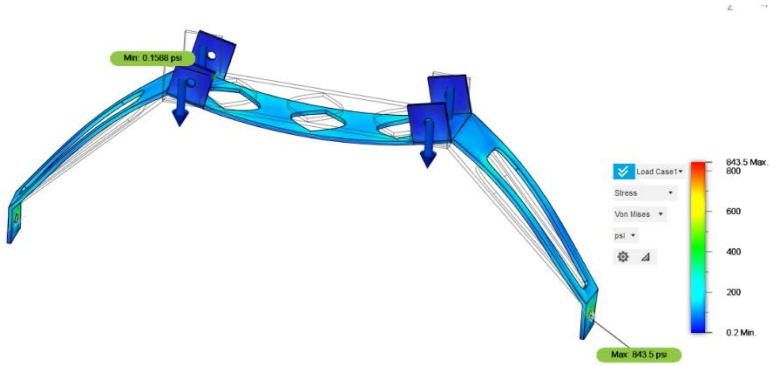

Figure 44: Fusion360 Deformation and Stress Analysis of Steel Bracket

Figure 45: Fusion360 Deformation and Stress Analysis of Aluminum Bracket

When designs such as the steel bracket prove to be ineffective, they are altered and re-tested until they satisfy the needs of the aircraft, as shown with the aluminum bracket.

FEA testing was also done on individual parts with high importance, such as the wing mounting brackets and locking brackets, to ensure that they would not fail during the high loading applied during flight. Failure in these parts could potentially result in total aircraft failure, and therefore they underwent rigorous testing and numerous alterations before their final iterations. The stress analysis of these parts can be seen in Figures 46 and 47.

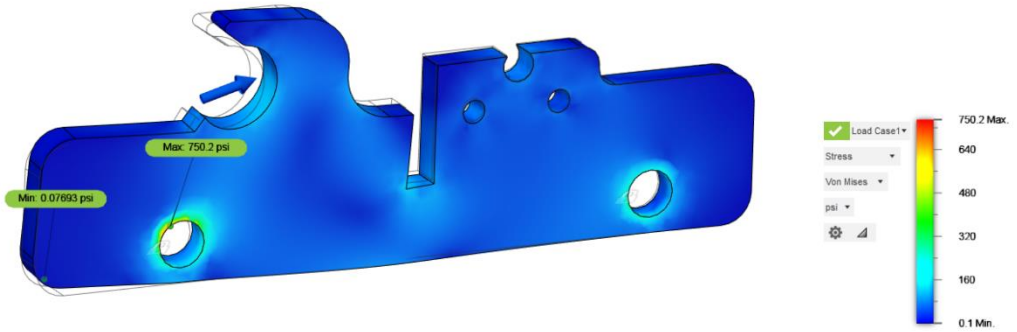

Figure 46: Fusion360 Deformation and Stress Analysis of Wing Mounting Bracket

Figure 47: Fusion360 Deformation and Stress Analysis of Wing Locking Bracket

The first major physical structural test performed was the aircraft drop test. The fuselage in Figure 48 was dropped from heights of two, five, and seven feet, and examined for structural damage. At the seven-foot height, the corners of some bulkheads sheared free, releasing some of the carbon spars. This resulted in a revised bulkhead design, increasing the tolerances between the bulkhead corners and the spars, and the new fuselage iteration survived the 7-foot drop height.

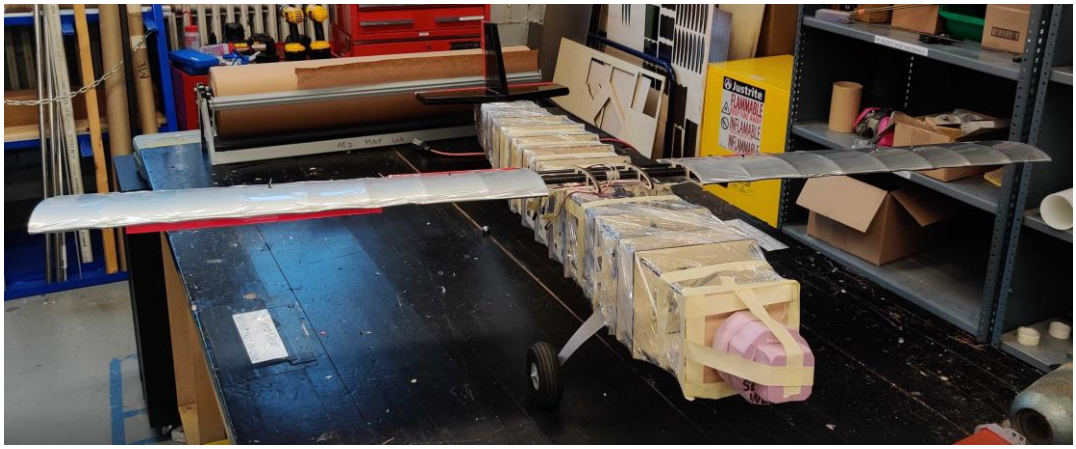

Figure 48: Fuselage Prior to Drop Testing

6.3.1 Payload Drop Mechanism

The testing of the preliminary payload drop mechanism design was conducted by using the transmitter to close the payload door, placing the simulated payload in the bay, then using the transmitter to open the payload door, deploying the payload. During this testing, it became apparent that the servo did not have sufficient torque to hold up the payload reliably, and the payload would also often get stuck between the partially open door and the walls of the aircraft.

The payload drop mechanism was redesigned as a result, instead lowering the payload straight down out of the aircraft. This payload mechanism was also tested, with the team ensuring that it could hold the payload's weight, raise and lower the platform with the payload, deploy the payload without setting off the shock sensors, and then retract the platform back into the aircraft. Figure 49 below shows the testing of the first iteration of the redesigned payload mechanism in comparison to the final version used at the competition. One prototype payload drop mechanism was built in a fuselage section, then both were held over a workbench at their estimated final height. The payload can be seen lowering with the platform, held upright by the pink foam sleeve mentioned previously, before exiting the aircraft and tipping over, falling the remaining 2 inches. These falls, unlike the falls from the full height with the door design, did not set off the shock sensors. Additionally, the platform was easily able to retract back into place without getting twisted or caught.

Figure 49: Testing of Payload Drop Mechanism

At the DBF competition, further testing and ground mission attempts indicated that the payload drop mechanism still dropped the payload too roughly. The team attempted the ground mission three times before successfully completing it. On each of the unsuccessful attempts, one sensor on one package was set off, often a result of the package falling off the door before reaching the ground and landing with too much downward or rotational force. After several iterations, the team was able to successfully deploy both payloads without setting off any sensors, completing the ground mission. The lower three images in figure 49, above show the payload lowered, resting on the line wrapped around it, then pivoting over that line, and finally resting on the ground after a gentle and successful landing.

6.4 Aerodynamics Testing

To ensure the aerodynamic quality of the aircraft when assembled the entire aircraft was modeled in XFLR-5. The VLM2, or ring vortex method was used to ensure that the fuselage and wing simulation paneling would not conflict or cause inaccuracies within the simulation. Streamline and stability testing was completed on the final configuration of the aircraft, and it was determined that nearly identical results were produced despite the slight center of gravity change from previous versions. The Figure 50 below includes the raw weight data for each "point mass" or sub-assembly.

Additional Point Masses

	Mass (kg)	x (m)	y (m)	z (m)	Description
1	1.300	0.000	0.000	0.000	6 vaccine vials
2	0.700	0.050	0.000	0.000	batteries
3	0.200	-0.200	0.000	0.000	motor

Figure 50: Point Mass Data from XFLR-5

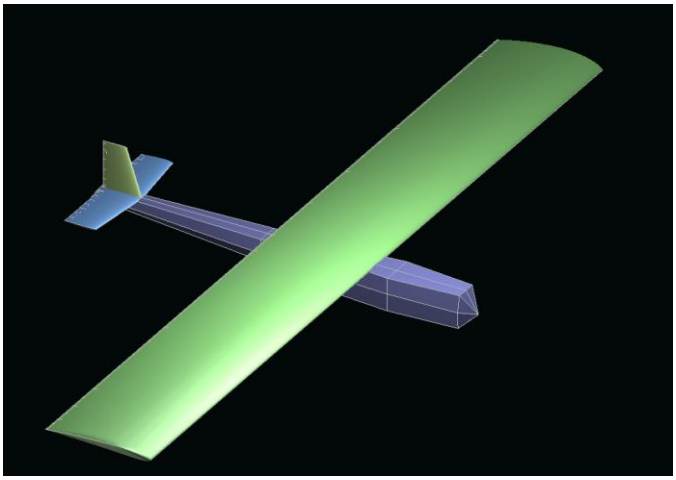

Figure 51: Airplane Fully Modeled in XFLR-5

The XFLR5 aircraft, pictured in Figure 51 above, was passed through several stability tests like the configurations before it. Much like the other configurations the aircraft was stable for all except for two conditions the phugoid mode and Spiral Mode. The eigenvalues for these

two conditions were slightly positive, indicating slight instability. Ultimately, the team determined that the eigenvalue was close enough to zero to cause significant alarm as slight instabilities can be trimmed for when in-flight. Table 20 below shows the stability values for each of the various modes.

Table 20: Stability Values

Stability Modes	Results
Phugoid Mode	0.0070 +-0.6827i
Short Period	-5.0317 +-7.9455i
Roll Convergence	-50.7947 +0i
Spiral Mode	0.1407 +0i
Dutch Roll	-0.9952 +-4.9147i

Further CFD testing was then done in SOLIDWORKS Fluid Simulation applet. Test conditions in SOLIDWORKS were kept as similar as possible to the conditions in XFLR-5 with similar masses, pressure and the same velocity of 22 m/s. Specifically, the CAD model assembly of the entire aircraft was put through several final CFD tests including particle mapping, streamline plotting and pressure gradient mapping. In Figure 52 of the SOLIDWORKS Fluid simulation, the green arrows indicate the average flow trajectory for the lifting surfaces, the green markings on the wing and in the background indicate that the aircraft, even in its simplified CAD version, can fly at 22m/s and stay stable within reasonable pressures.

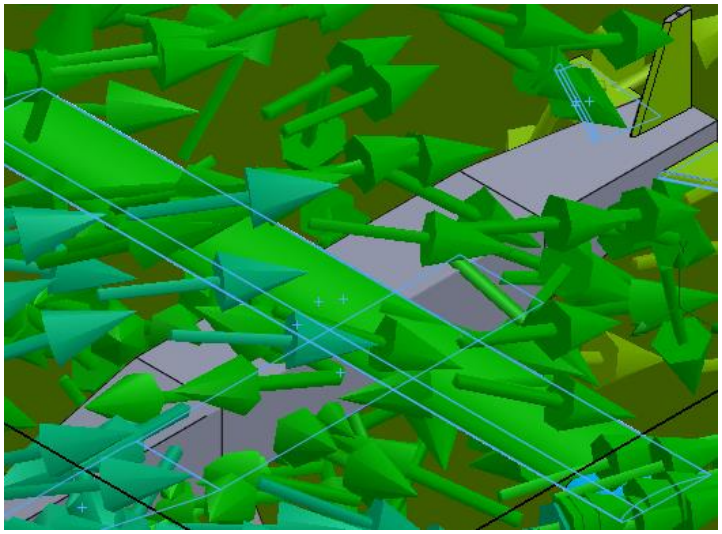

Figure 52: Flow Simulation Pressure Gradient and Flow Trajectory

After confirming the validity of the cruise speed prediction, the team began the building and in-depth design process.

6.5 Controls Testing

The controls subsystem was tested frequently to ensure that each servo was capable of smoothly moving its control surface the correct amount in the correct direction when actuated by the pilot. Since the ailerons and flaps are on separate channels, with outputs 2 and 3 from the receiver going to the left and right aileron respectively and outputs 6 and 7 going to the left and right flap respectively, it was essential that each control surface was confirmed to be operating correctly before any other testing or flying. For the control surfaces on the wing, the ailerons were tested to confirm that they were centered when receiving no roll input from the transmitter, then to confirm that they moved in similar amounts and in opposite directions when the pilot moved the roll axis. When the pilot moved the right stick of the transmitter to the right, the right aileron was confirmed to raise and the left aileron to lower. The flaps were linked to a 3-position switch on the transmitter and were tested to confirm that they moved together and were in similar positions at each switch position. On the tail, the elevator was tested to ensure that it responded correctly to elevator inputs and had appropriate deflection. As can be seen in the detail design section for the tail, the rudder was cut to allow full elevator deflection.

6.6 Overall Aircraft Testing

Before this report's completion the team conducted numerous powered flight tests, 3 glide tests and numerous physical tests like the drop tests mentioned above. Below, Tables 21 and 22 show the process the team follows prior to each test to ensure that the aircraft was in good condition and was safe to handle and fly.

Table 21: General Requirements Checklist

Subsystem	Step	Description	Pass	Fail
Fuselage	1	Fuselage is free from cracks		
	2	Monokote is not torn or detached		
Wing	1	Wing is solidly attached to fuselage		
	2	Flaps and ailerons function properly		
	3	Monokote is not torn or detached		
Tail	1	Tail is solidly attached to fuselage		
	2	Elevator and rudder function properly		
Landing Gear	1	Landing gear is secured to aircraft		
	2	Main wheels spin freely		
	3	Tailwheel spins freely and steers		
Aircraft	1	Check that lateral and longitudinal CG are correct		
	2	Wingtip test to ensure overall aircraft rigidity		

Table 22: Component Checklist

Component	Step	Description	Pass	Fail
Transmitter	1	Transmitter battery is charged		
	2	Correct model selected		
Receiver	1	Ensure all wires in correct channel and fully connected		
	2	Battery telemetry sensor connected to battery		
	3	Conduct range test to confirm connection		
Motor	1	Motor is secured to fuselage		
	2	Inspection of wiring to ESC		
	3	Motor spins correct direction		
Propeller	1	Propeller secured to motor shaft		
	2	No damage to propeller leading edge or tip		
Battery	1	Battery fully charged		
	2	Inspection of wiring to ESC		
Fuse	1	Check fuse unbroken		

7 Performance Results

7.1 Subsystem Performance Results

7.1.1 Propulsion

To perform analysis on the propulsion set-up, the team did experiments using a thrust stand at static and constant airspeed conditions. The team tested the propulsion set up with both propeller configurations as well, the 15x7x3 as well as the 15x4. During these tests the team collected performance metrics such as current entering the motor, voltage of the battery as well as total thrust output of the motor. The expected values come from the data sheet provided by Scorpion, the manufacturer of the selected motor and ESC. At full throttle the team expected the 15x4 propeller and motor to produce 7.76 pounds of thrust with an input voltage of 14.8 V and an input current of 42.51 A. For the 15x7x3 at full throttle the team expected 10.69 pounds of thrust with an input voltage of 14.8 V and an input current of 75.65 A.

To measure the thrust of the motor, the team used the RCBenchmark 1585 Thrust stand. This thrust stand allowed for the mounting of the motor to the front using size 6 screws with locknuts to eliminate unwanted vibration. The team then attached the electronic speed controller, receiver and battery to the motor making sure to tie them down to reduce any vibration inside the safety cage. To measure the thrust the team used the corresponding RCBenchmark software, which can be connected to the stand via a USB cable. To measure the performance of the motor, or the current, voltage, revolutions per minute and throttle input, the team used the software for the Scorpion Tribunus II electronic speed controller, called Sproto. The software required a connection via a USB cable to the side of the electronic speed controller. An important note was that the team set the maximum input amperage of the electronic speed controller to 95 A, or the total the motor was able to handle. When values were programmed into the electronic speed controller that were lower than this it throttled the amperage from the throttle and gave lower values than expected. To achieve full thrust, setting the electronic speed controller to 95 A was required.

The first experiment that was run to analyze the propulsion system was the static thrust test. This test was done using the set up seen in Figure 41 of Section 6.2. Data was collected for the input current, input voltage and the total thrust from the motor. This data was organized for

each propeller into a table that the team used to create two plots. The first plot was the thrust versus input current of the motor, which can be seen below in Figure 53.

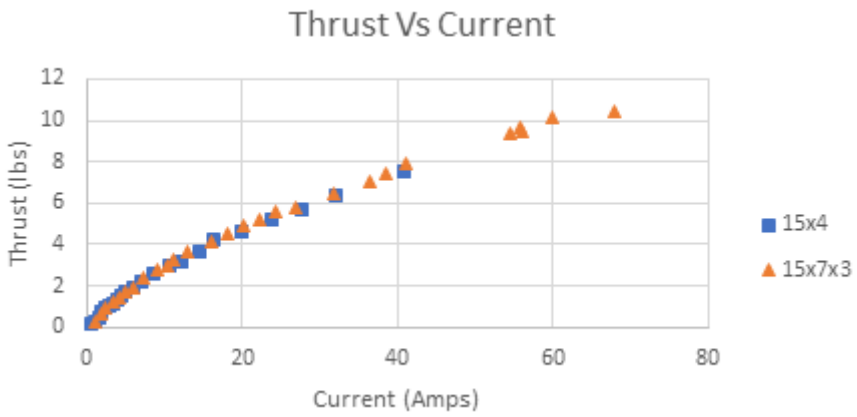

Figure 53: Plot of the Thrust vs. Input Current for both propellers

One important conclusion from the data in Figure 53 was the maximum constant thrust and endurance can be retrieved from each propeller setup. Looking first at the 15x4 propeller the team measured a maximum thrust of 7.51 pounds. This was extremely close to the 7.76 pounds of thrust that was predicted from the data sheet given by Scorpion. The missing 0.25 pounds could be attributed to difference in temperature or altitude of testing that could affect air density or possible difference in battery or electronic speed controller. The equation for thrust of a propeller can be seen below as Equation 7. From this equation it can be shown how air density ρ can influence the total thrust of the aircraft. It can also be concluded from this data that at maximum thrust it requires and input current of 40.9 A. Since the battery had a capacitance of 6500 mAh which can be discharged up to 85%, the aircraft endurance was 8.07 minutes when the motor spins at full throttle. This was enough endurance to complete a 10-minute maximum Mission 3 assuming over 2 minutes minimum of landing and package dropping time.

$$Thrust = \frac{1}{2} A\rho({V_e}^2 - {V_0}^2) \tag{7}$$

For the 15x7x3 propeller a maximum continuous thrust of 10.48 pounds was calculated. This value was lower than the expected value of 10.70 pounds of thrust from the Scorpion data sheet. This decrease of 0.22 pounds in thrust was similar to losses in the 15x4 propeller. A

difference in air density could account for drops in both propellers as the tests were done at the same location. A slight decrease in performance of the motor compared to the one used the manufactures testing was possible as well. At the maximum thrust of the 15x7x3, it required an input current of 68.0 A. This would correspond to a flight time of 4.82 minutes which gives far more time than needed at the predicted and calculated airspeed to complete the flight of Mission 1 and 2 at the fastest possible time and greatest payload.

The next plot that was created with this data was thrust versus the total input power. The power was calculated as the current times the voltage to get power in Watts. The plot can be seen below in Figure 54.

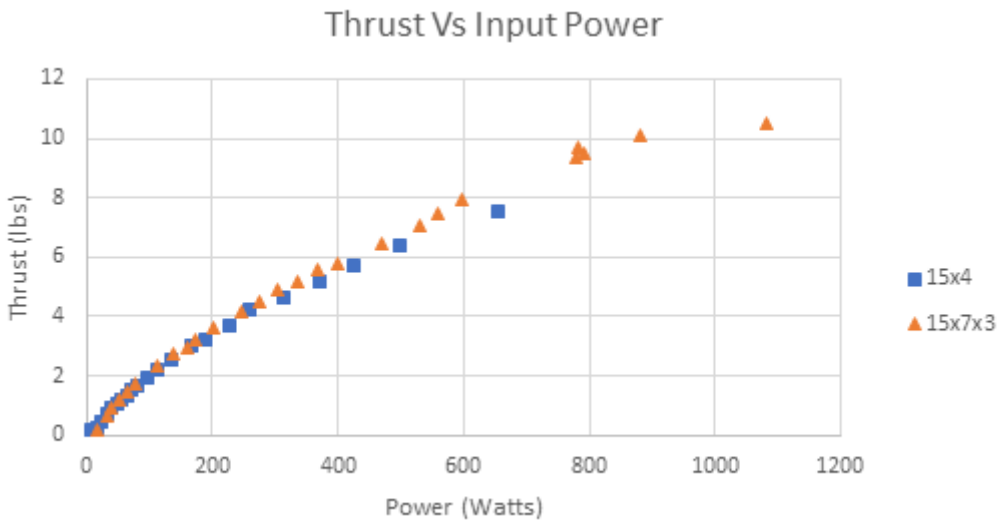

Figure 54: Thrust versus the Total Input Power of The Motor for each Propeller

The plot in Figure 54 shows how the voltage of the battery affects the slope of the curve. When comparing this to the plot of thrust versus current extremely smooth lines are found. From 0-15A a slightly non-linear pattern was present in comparison to the strong linear pattern seen from 15-68. For the thrust versus power curve, more variation exists between points. In the thrust versus current plot, the lines overlap almost the whole time. However, for the thrust versus power at about 300 Watts, a variation in propellors starts to occur and the stronger 15x7x3 propeller provided more lift. This was expected as the 15x7 had more pitch than the 15x4 which meant more thrust was produced, validating the curve.

Another test the team ran was a propulsive test in variable airspeed conditions. Data was collected for thrust at different throttle and current values and plotted these lines versus the static condition. The team chose to use air speeds of 10 m/s and 15 m/s to try and estimate the flight speed of the aircraft. At higher airspeeds the difference in airspeeds from before and after the propeller were going to be much lower with an incoming airspeed greater than 0 that of static. This resulted in a loss of thrust which was displayed in the experimental results. Equation 5 above explains this difference, as thrust is caused by the difference between ambient and exit velocities. The maximum thrust of the 15x4 propeller at static conditions was 7.51 pounds, however with airspeeds of 10 m/s and 15 m/s a maximum thrust of 4.84 pounds and 3.96 pounds was calculated. This can be seen in Figure 55 below.

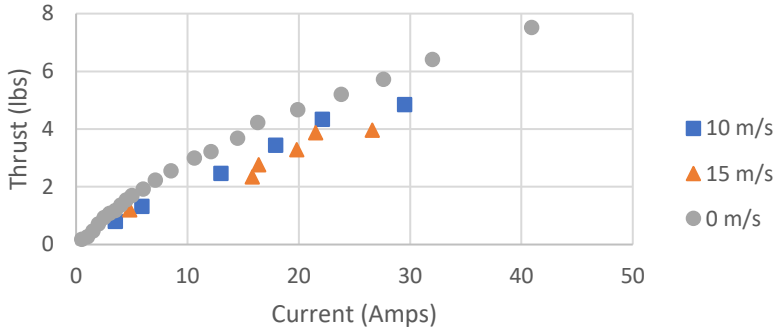

Figure 55: Thrust versus Current at Various Airspeeds for 15x4 Propeller

7.1.2 Structures

The aircraft experienced multiple crashes upon during flight test, which served a performance metric for the structural subsystems of the aircraft. The impacts were primarily focused on the nose and middle fuselage, which typically damage. The Carbon fiber rods survived the impact without damage, and any damaged bulkheads within the central fuselage were easily replaceable. The final landing gear design was able to withstand rough landings without shearing or deforming. The original plan for the wing attachment featured a series of pins and a top-down locking bracket. 3D printed versions of the bracket were replaced by plasma-cut aluminum versions to ensure maximum strength and failure resistance.

7.1.3 Aerodynamics

Aerodynamics testing started in the WPI wind tunnel. The team 3D printed a subscale section of the wing, a NACA 4412 airfoil 3.26 in by 5 in was tested. Equation 6 below was used to find the lift produced by the wing prototype.

$$L = N * \cos(AOA) \tag{8}$$

While the wing was mounted at an angle of attack (AOA) of zero degrees, the team anticipated the aircraft would fly with an AOA of 2-5 degrees. Calculations with the wind tunnel data confirmed that the wing produces enough lift to support the aircraft and the loads it was subjected to during flight. The aircraft was estimated to weigh 8 lbs. and was expected to sustain loads up to 2.5x its weight. At an AOA of zero, the wing produced 5 lbs. of lift. This value increases with the AOA until an angle of 12.35, producing 13 lbs. of lift.

After the wing was assembled and secured to the aircraft, it was tested in flight. The wing worked as expected, creating enough lift to get the plane off the ground. The flaps and ailerons also worked well and did not inhibit the wing's ability to fly the aircraft. Even so, changes were made to the location of the wing to better suit the location of upwards forces produced, due to complications describes in the controls section below.

7.1.4 Controls

In the initial unpowered glide tests, the controls subsystem performed as expected, allowing the pilot to make minor corrections to the aircraft's pitch to correct for initial pitching up or down at launch. At this point, no improvements were made.

During the first powered flight test at the WPI track, the controls subsystem did not perform adequately. The aircraft pitched up dramatically immediately after takeoff and rolled to the left, nearly hovering for most of the 20 second flight before entering a shallow flat spin and crashing at a slightly nose down angle. Despite the CG being confirmed to be in the correct location before the flight, the aircraft appeared to fly as if it was extremely tail heavy, so the tail was redesigned to double the size of the elevator and add approximately 3 inches to the vertical stabilizer. This dramatically improved pitch and yaw stability. One potential cause of this could be the XFLR-5 and SOLDIWORKS analysis not including disruptions to the airflow over the tail

caused by the fuselage. To further increase the stability, the aircraft's CG was moved forward for the next test flight. The old tail can be seen next to the in-progress redesigned tail in Figure 56 below.

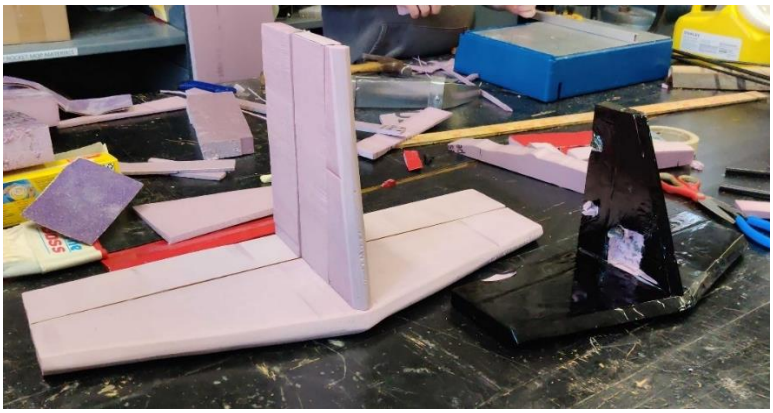

Figure 56: Redesigned Tail Compared to Old Tail

During the second powered test flight, the aircraft was flown from the WPI track. Over multiple attempts, the aircraft didn't lift off the ground, partially due to the elevator and rudder pushrods slipping followed by the elevator control horn breaking free from the elevator. Additionally, the angle of attack during attempted takeoff was much lower than in the first test flight due to the aluminum landing gear, causing the aircraft to not develop enough lift to take off. To address this, the pushrods and control horns were replaced.

In the third powered take-off flight, the aircraft was flown from an elevated concrete surface at a nearby park to test the new landing gear. The flight was intentionally more of a hop than a full flight as there was not enough room or daylight for a full flight. Takeoff was attempted from the grass, but due to the new landing gear including a pivoting tailwheel, the aircraft would turn to the left while taxiing on the uneven grass surface. As can be seen in the six images below in Figure 57, the aircraft pitched up and rolled to the left during the short flight, indicating that the aircraft was still tail heavy. The throttle was ramped up to full before image 1 and was cut off to zero around image 4 to set the aircraft down in the grass.

Figure 57: Images from Take-off Test Flight

8 Aircraft Performance Testing

8.1 Glide Test

The first performance test that was conducted was a glide test. This was conducted in Alden Hall in the main auditorium. The aircraft had the core electronics in place, including the motor and battery to achieve an approximate CG, but the propeller was removed, and the motor was disconnected and covered with foam to protect from damage. Supplies such as tape, weights, and other material were utilized to shift the CG to the correct location. The elevator and ailerons were controlled during the flights by the pilot, but the flaps and rudder were fixed in place. The team elected to utilized saran wrap for an aerodynamic surface on the fuselage to negate the unneeded loss of MonoKote. This experimental configuration can be seen in Figure 58 below.

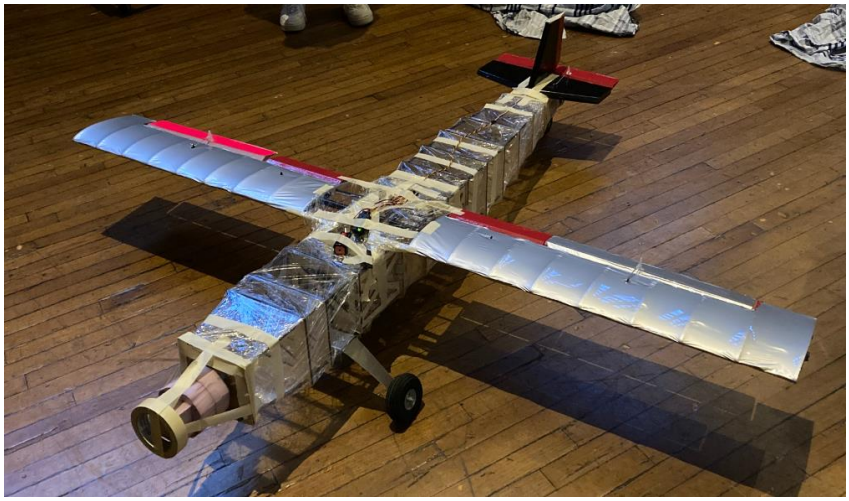

Figure 58: Glide Test Experimental Set-Up

The first test was roughly 10 feet off the ground to make sure a larger glide would work. Once this was completed the team used the top balcony to drop the aircraft in a glide from roughly 25 feet. This test went extremely well, and the aircraft travelled roughly 30 feet and the aircraft was caught it in a bed sheet to avoid damage.

8.2 Flight Test 1

The first Flight test was conducted at WPI's Alumni Field and suffered from a few issues. The flight can be characterized as an uncontrolled hover. The flight started with a 42 foot take off and then entered a quick bank to the left. The aircraft went into an uncontrollable vertical

climb. Still shots of the aircrafts flight test can be seen below in Figure 59, demonstrating the lack of air performance for this iteration of the aircraft. The first still, reading from top left to right, one can see the aircraft immediately bank left upon take off. The aircraft then proceeded to continue with the bank left until it was in a complete hover showcased in the second and third still. After cutting propulsion due to the aircraft approaching the Recreation Center, the aircraft proceeded to move towards the ground. Although the aircraft crashed, the control surfaces allowed the plane to have a controlled crash, validating the controllability of the vehicle. The flight video can be found in the attached compressed folder to the MQP report.

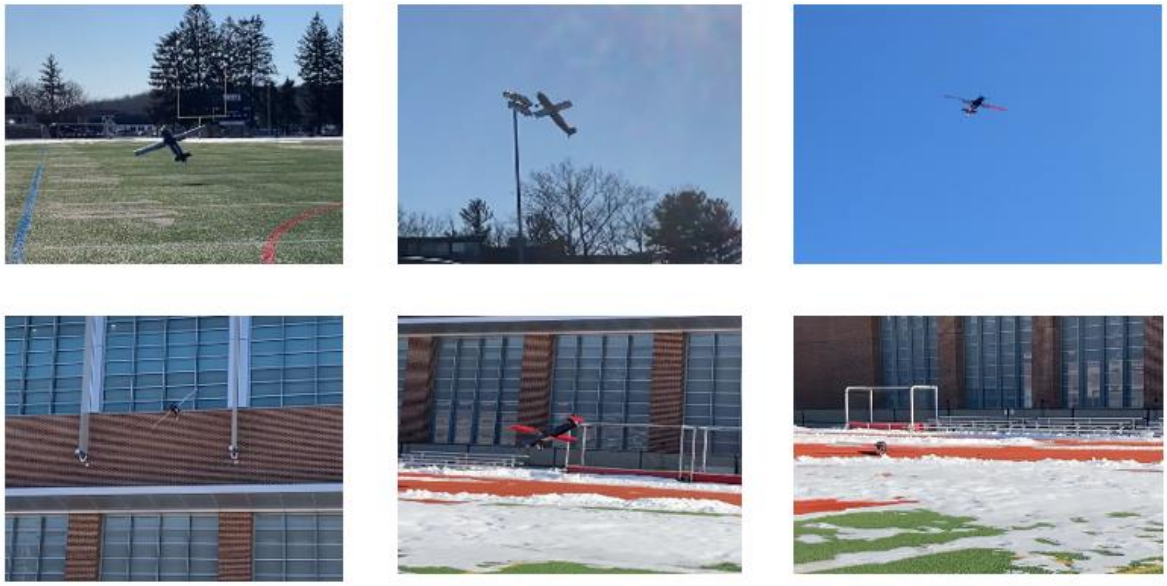

Figure 59: Still Shots of the Aircraft During Flight Test 1

A few issues were identified from this flight. The first being aerodynamic flow issues. The aircraft had a very square structure to the fuselage with the motor mounted directly on the front. This caused a large amount of the accelerated flow from the propeller to become turbulent and get dispersed by this bulkhead. To fix this issue, the team decided to increase the entire tapering to the front of the aircraft as well as add about 6 inches to the front in length. This change can be seen in Figure 60. One can identify a significant taper when comparing the left version (flight test 1) to the right version (flight test 2).

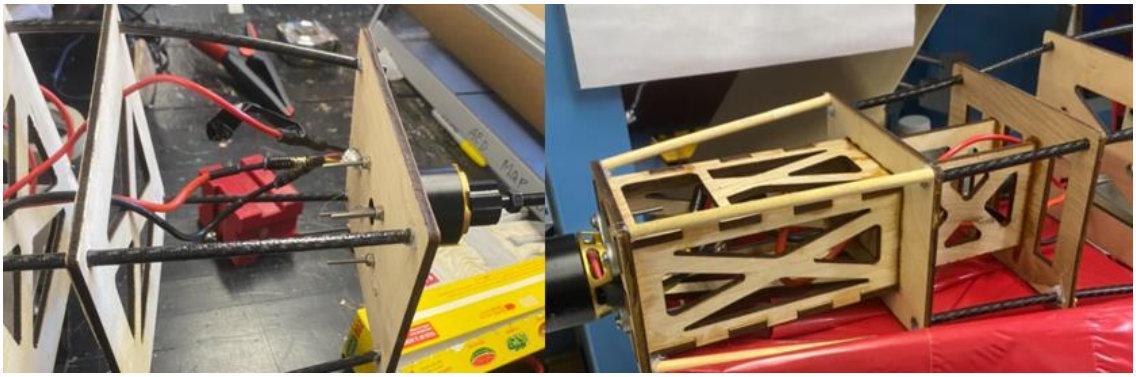

Figure 60: Comparison of Front Tapering Between Flight Tests

This led to a total reduction of the front bulkhead by an inch on each side and a total fuselage length of 66 inches. The next and possible largest issue from this flight was the uncontrollability and uncontrolled climb or hover that was experienced. This was due to a lack of lift and trim from the tail of the aircraft. To fix this issue the size of the tail was doubled but the same 0012 airfoil shape was kept. The horizontal tail area went from 81.77 in^2 to 163.54 in^2. The vertical tail area went from 36.95 in^2 to 73.9 in^2. The last issue that came up was that the center of gravity was not where it was intended to be. This led to a change in where the wing was attached to the fuselage of the aircraft.

8.3 Flight Test 2

The second flight test had a dissimilar experience than the first flight and did not take off at all. The aircraft picked up speed on the ground but just rolled along the track and was unable to take flight. This was the fault of over design. Far too many variables were changed at one time and made backward progress on the aircraft. The flight video can be found in the attached MQP folder. The second flight test configuration of the aircraft can be seen in Figure 61 below. The largest issue this flight had was the obvious lack of takeoff. The second was a lack of steering from the fixed landing gear.

Figure 61: Flight Test 2 Aircraft Configuration

The easiest fix from the previous flight to fix was the lack of steering from the aircraft. To solve this, the team purchased a Sullivan tailwheel bracket which was controlled by one single servo motor. This was installed in the back of the aircraft. To solve the takeoff problem, the team needed to balance changes to the aircraft to increase lift while removing some of the previous changes. The first change made was to keep the front tapering but removed the extra length added to the fuselage. This kept the solution to the aerodynamic flow but reduce weight and length of the aircraft. The second thing changed was the use of the 15x4 2 blade propeller rather than the 15x7 3 blade previously used. While the 15x4 propeller theoretically still had a great thrust to weight ratio, due to the inability to takeoff it was decided to use the 15x7x3 propeller to maximize thrust at takeoff. The team also improved the landing gear by designing a custom steel landing gear to angle the aircraft at 11 degrees, the calculated optimal angle of attack. In addition, the team laser cut removable wing attachment brackets with various angles of attack, to allow testing of various wing locations and angles.

8.4 Flight Test 3

The third flight test was the first of many remarkably successful flights. The flight started with a 45-foot take-off followed by extremely stable flight and a successful landing. The total flight time was 56 seconds, and no power loss was encountered during the time of flight. The aircraft was able to complete the 360 degrees turn with no issue and with no flaps. The third configuration of the aircraft can be seen in Figure 62.

Figure 62: Flight Test 3 Aircraft Configuration

The main issue with this flight was the fact that it had a 45-foot takeoff distance while the maximum for competition was 25 feet. Still shots of this flight can be seen in Figure 63.

Figure 63: Still Shots of Flight Test 3

Another issue that was necessary to address was the lack of auto leveling due to the flat rectangular wing. To address the takeoff distance, first the team wanted to remove weight that was unnecessary, so the payload bay was removed making the total payload capacity for mission 3 only four payloads. The team also added a larger tail wheel to hopefully remove friction while on the ground. The chord length of the main wing was also increased by 0.5 inches via the addition of larger flaps on the aircraft. The biggest change that was made for the next flight was

the addition of 6-inch wing tips with 25 degrees of dihedral to try and increase the stability of the aircraft in flight.

8.5 Flight Test 4 & 5

Flight test 4 and 5 were both unsuccessful and resulted in the destruction of the aircraft on both attempts. The new dihedral wings were flown during the fourth flight test. Figure 64 shows the added dihedral and wing tip size. The dihedral was created utilizing a 3-D printed elbow joint that locked into the current carbon fiber spar and extended 6 inches using an additional carbon fiber spar.

Figure 64: Dihedral Wing

This flight had a 25-foot takeoff distance however once in the air was unable to turn due to being overly stable. It was particularly challenging to turn and resulted in a crash that broke the wing and many bulkheads in the aircraft.

After flight test 4 the team wanted to keep the great takeoff distance that would put us in compliance with the mission requirements but keep the old stability. This led us to increase the wing by a total of 1.5 feet to a total 7.5 feet just under the 8-foot maximum dimensions in the competition rules. Larger flaps were created adding an additional 0.5 inches to the chord length. When adding length to the wing one receiver was also placed on the main spar of the wing.

Flight test 5 was the first test completed with the changes added to the aircraft. This flight had a great takeoff distance averaging about 20 feet on small hops. However, when a full flight was attempted, the pilot lost connection with the plane and it made a banking left hand turn into the ground. This resulted in a destruction of the wing and many of the bulkheads in the fuselage. The main carbon fiber spar in the fuselage was also lost in the crash. A picture of the aircraft after the crash can be seen in Figure 65 below.

Figure 65: Flight Test 5 Crash

To remedy this issue, the antennas of the receiver sticking outside of the aircraft, so the loss of connection was not a possibility. The carbon fiber spar was repaired with epoxy as well as a fiber glass wrap. This worked very well and held exceptionally for all further flight testing and competition.

8.6 Final Flight Iterations

After flight test 5 changes were implemented and the placement of the receiver the aircraft was now in its final configuration. With all the changes from the first flight the aircraft now had a 15-foot takeoff unloaded and an 18-foot takeoff with the maximum amount of payload. The flight speed of the aircraft was measured to be 15.61 miles per hour. The flight speed was calculated by measuring 30 feet in a straight line and marking both ends. The team then took 3 times from different vantage points to try and eliminate human error and parallax. This led to an average time of 1.31 seconds which corresponds to 22.9 ft/s or 15.61 miles per hour. Still Shots of the final flight prior to competition can be seen below in Figure 65.

Figure 66: Still Shots of the Final Flight

9 Outcomes and Conclusions

9.1 Competition Outcomes

On April 20th, 2022, half of the Design Build Fly Team flew out to Wichita Kansa for the DBF competition. When the team arrived, a wind advisory was immediately placed into effect. On the first day of the competition the team passed the tech inspection allowing us to qualify to participate in ground and flight mission attempts. The aircraft was able to pass the inspection on its first try thanks to the simple wiring, pre-established failsafe conditions and solid fuselage and wing construction. On Friday, the team attempted a flight of Mission 1 while the wind advisory was still in effect, the aircraft flew in wind speeds averaging 37 mph and gusting at 55-60 mph. The wind was so strong at certain moments during the flight that when faced with a gusting headwind the aircraft was unable to overcome the speed of the wind and effectively hovered in place for nearly 2 minutes. Due to the wind gusts, the aircraft touched the ground after take-off, and it unfortunately failed this attempt due to competition rules. However, it is imperative to note the stability and overall airworthiness the aircraft displayed in these conditions. The image in Figure 67 below shows the stability and the hovering of the aircraft during the first attempt of Mission 1.

Figure 67: Mission 1 Attempt

(Photo Credit: Gage Kuszmaul, Clarkson University)

After this flight attempt the team took to attempting the ground mission. Over the course of Friday afternoon and Saturday morning the team attempted and failed the ground mission 3 times setting off the vaccine vial sensor each time. After making improvements to the payload bay, the team member and the aircraft were able to complete the ground mission in 2 minutes and 16 seconds. On the last day of the competition Mission 1 was attempted 1 more time. On the turn before the final lap however, the aircraft lost thrust seemingly for no reason at all. The team later discovered that either a relay or a mosfet chip inside of the ESC failed to function causing the ESC to lose sync with the controller, causing a final failure which proved to be non-repairable. It should be noted that the aircraft was able to safely glide to a landing on the runway despite the loss of engine power.

9.2 Conclusions

During the 2021-2022 AIAA DBF competition, the team successfully passed the tech inspection and ground mission, and the designed aircraft was able to fly in strong wind and even land safely with loss of power. It is important to note the aircraft's flight dynamics even in extremely poor flying conditions. When the team started the design process, a goal was set to design an extremely stable aircraft, which produces high lift and can take off within 25 feet. The aircraft not only achieved the goals set out to be achieved but was able to reliably carry 20 medical syringes or 2 vaccine vial packages. Ultimately, while some failures did occur the team was able to succeed in the goals set at the beginning of the year.

9.3 Broader Impacts

This aircraft had great potential to be scaled and used for many different humanitarian missions. The modularity along with the large payload capacity of the aircraft allows for quick and easy changes in the payload bay. For a mission such as bringing food to a natural disaster zone this aircraft would easily be able to change the payload bay to hold food rations instead of syringes that can be remote deployed to hard-to-reach areas. The aircraft had been shown to be extremely stable and pilotable so that even a beginner pilot would be able to help when the aircraft is deployed. The short take off would also be beneficial in a natural disaster environment if there was lots of debris to avoid on the ground. The quick configuration of the payload bay would be crucial for the design and deployment of many different future missions.

9.4 Future Work Recommendations

The aircraft designed by this year's team was a high quality and robust attempt to fulfil the needs of this year's DBF competition. The most valuable recommendations we can pass on to teams attempting the DBF competition in the future are the following. Do not squander the down time before the competition rules are released, you can prepare by brushing up on your knowledge of different software packages such as XFLR-5, ANSYS and Solidworks. It is imperative that the design report is started early, as the report is deceptively robust piece of writing which a good score can help propel you to a high scoring seed at the competition. Finally, do not be afraid to crash your aircraft. Repairs and redesigns can always be done quickly and efficiently. The 2021-2022 DBF Team would like to wish future teams good luck and to have fun at competition in years to come!

References:

[1] Chinwicharnam, K., & Thipyopas, C. (2016). Comparison of Wing–Propeller Interaction in Tractor and Pusher Configuration. *International Journal of Micro Air Vehicles*. https://doi.org/10.1177/1756829316638206

[2] Condit, R. (2004). Brushed DC Motor Fundamentals. *Microchip Technology Inc.* http://www.moderncontroltechnology.com/docs/DataSheets/Microchip/more_stuff/BrushedDC_MotorControl_AN905.pdf

[3] Daniel, R. (2013). *Aircraft Design*. American Institute of Aeronautics and Astronautics.

[4] Gao, K. (n.d.). Understanding Motor Turns & Kv Rating. *ATees*.

[5] Li, Y., Samantha, C., Almeida, M., Dimilia, M., Korza, A., Donahue, J., & Hlavenka, T. (n.d.). Micro Aircraft Design Dbf-2017. *Worcester Polytechnic Institute*.

[6] Ryan. (2018). Brushless Inrunner vs Outrunner motor? *Radio Control Info*. https://www.radiocontrolinfo.com/brushless-inrunner-vs-outrunner-motor/

[7] Schutes, J., Rosano, A., Kelly, M., Cashman, D., Tosi, N., Andraka, A., Di Christina, G., Sullivan, C., Pugilese, C., & Demers, Z. (2015). Design of a Micro Aerial Vehicle. *Worcester Polytechnic Institute*.

[8] Sharma, P., & Atkins, E. (2018). *An Experimental Investigation of Tractor and Pusher Hexacopter Performance*.

[9] Shoer, N., Bugdin, T., Trainor, J., Shriner, M., Teirlinck, D., Henehan, S., & Weaver, S. (2021). Design of a Fixed Wing Micro Aerial Vehicle. *Worcester Polytechnic Institute*.

[10] Smite, J., & Haughn, R. (2022). Lipo Battery Basics. *The Academy of Model Aeronautics*.

Appendix: Final Drawings

See next page for drawings

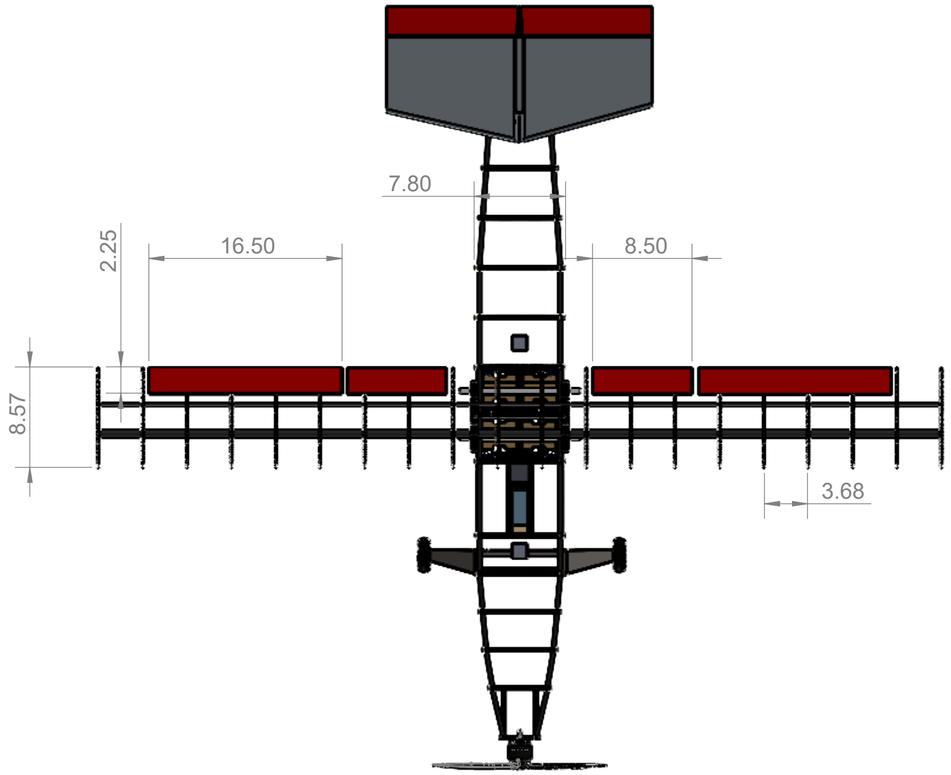

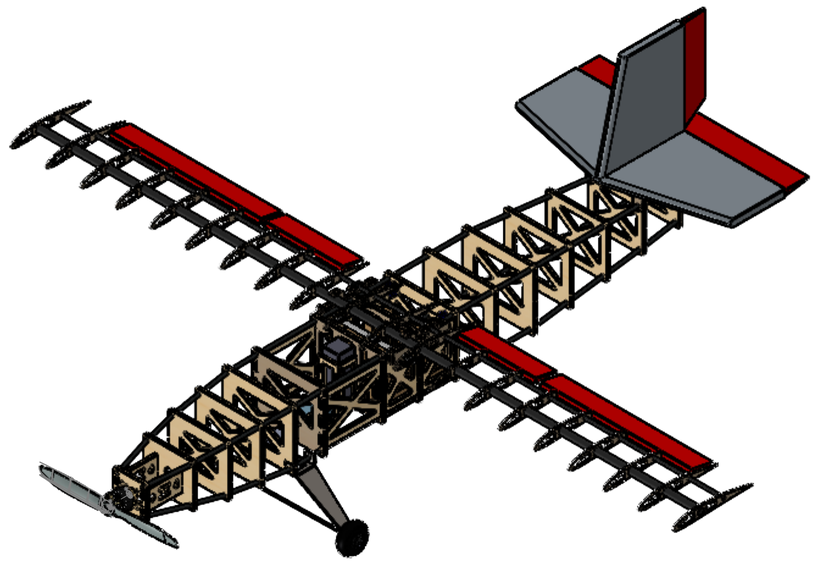

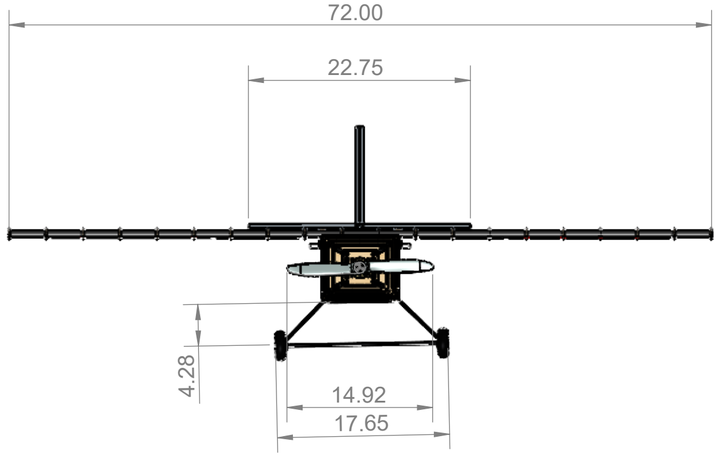

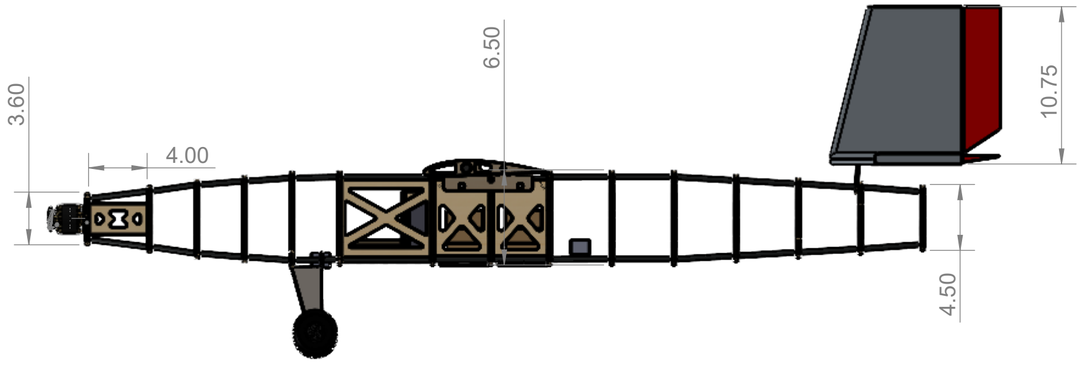

	NAME	DATE
DRAWN	JM	2/1/22
CHECKED	SV	2/2/22
ENG APPR.	BW	2/5/22
MFG APPR.	CD	2/6/22
Q.A.	JJ	2/7/22

COMMENTS:

Unit: Inches

UNLESS OTHERWISE SPECIFIED:

3 View Drawing

TITLE: Rude Goose

SIZE	DWG. NO.	REV
B	DBF_2022_WPI_Drawing 1	

SCALE: 1:12 SHEET 1 OF 2

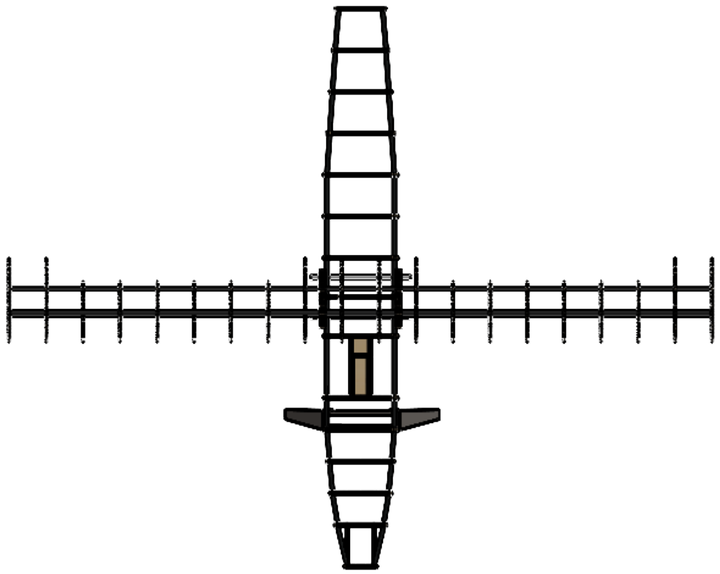

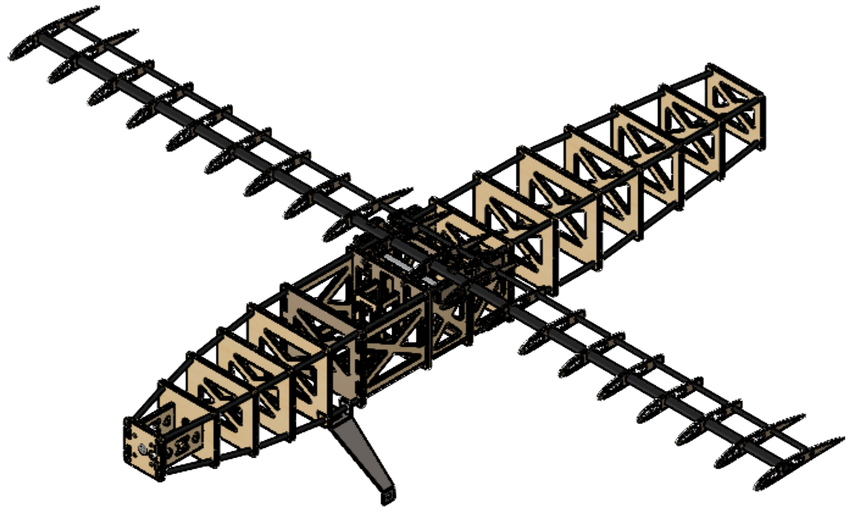

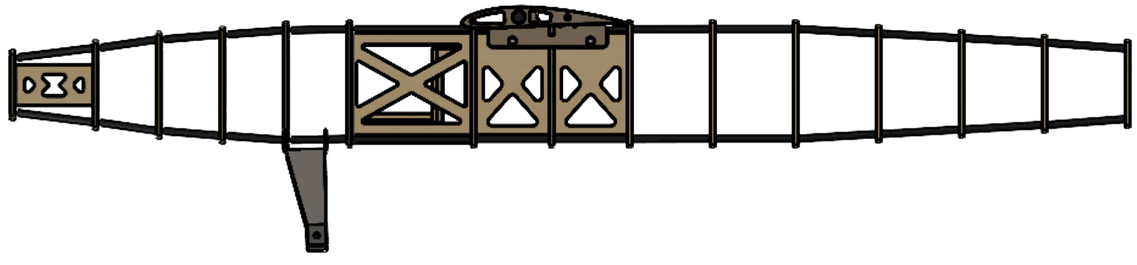

	NAME	DATE
DRAWN	JM	2/1/22
CHECKED	SV	2/2/22
ENG APPR.	BW	2/5/22
MFG APPR.	CD	2/6/22
Q.A.	JJ	2/7/22

COMMENTS:

Unit: Inches

UNLESS OTHERWISE SPECIFIED:

Structural Arrangement

TITLE:

Rude Goose

SIZE	DWG. NO.	REV
B	DBF_2022_WPI_Drawing 2	

SCALE: 1:12 | SHEET 2 of 3

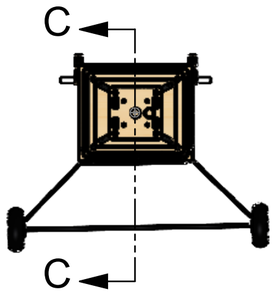

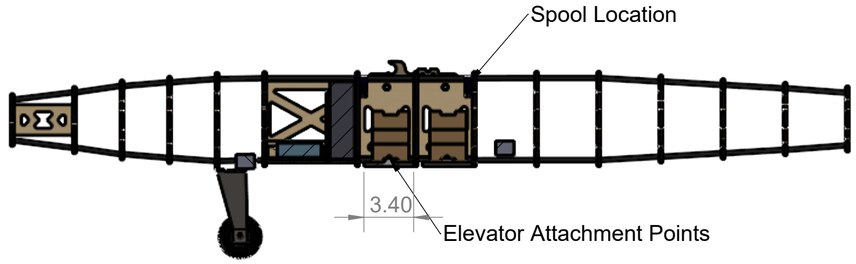

SECTION C-C

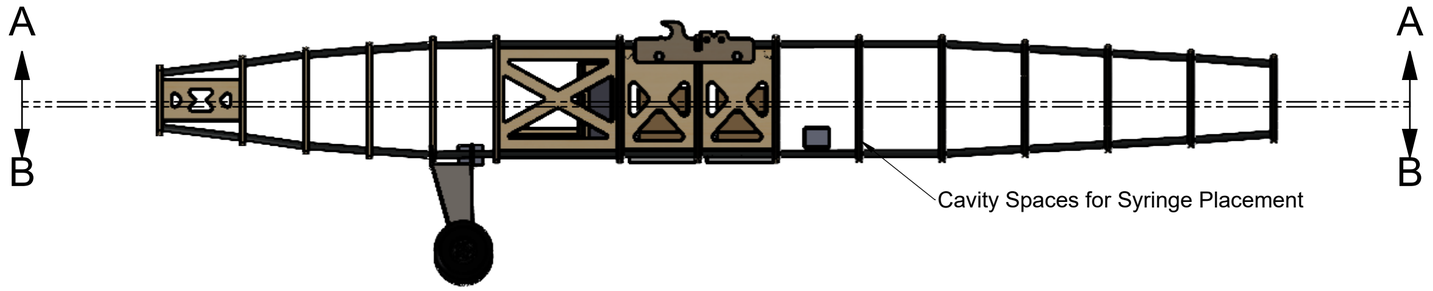

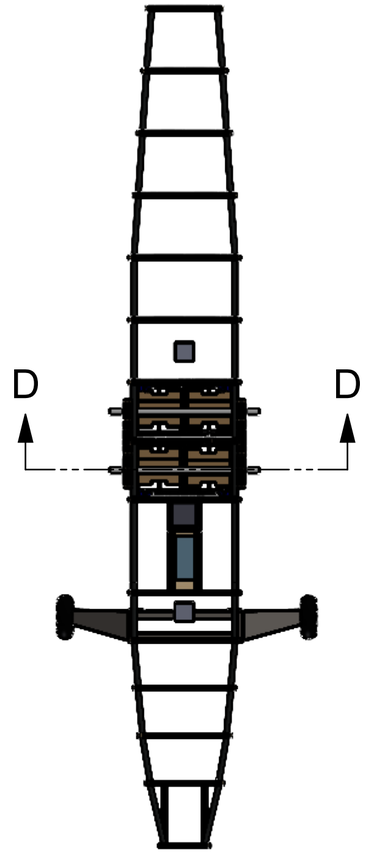

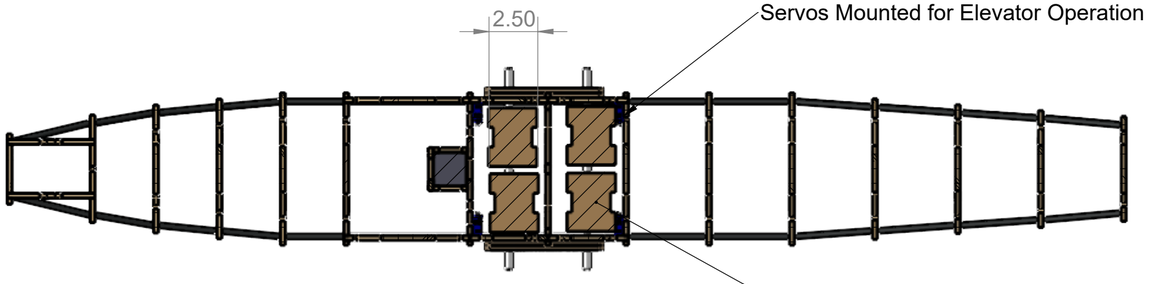

SECTION A-A

SCALE 1 : 6

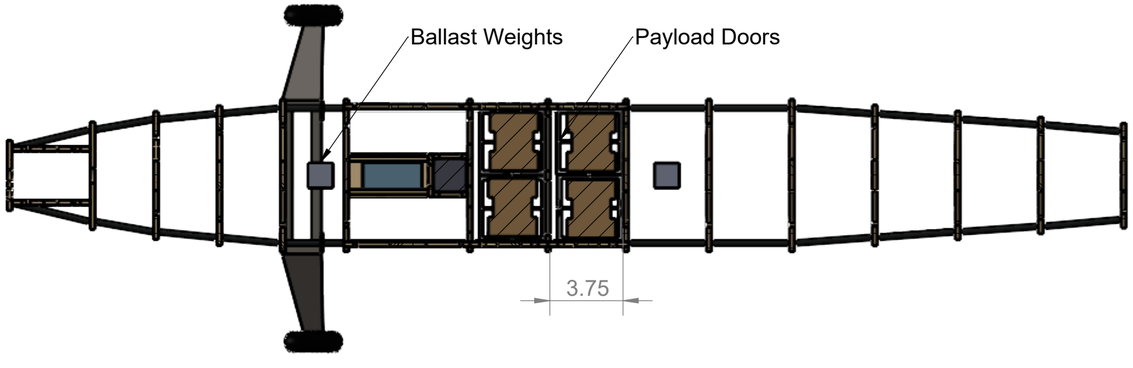

SECTION B-B

SCALE 1 : 6

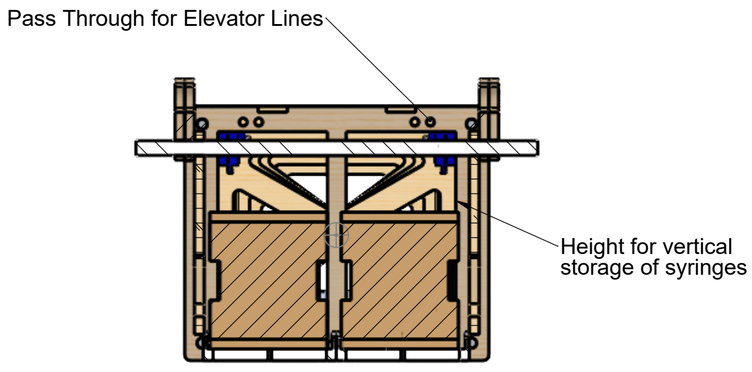

SECTION D-D

SCALE 1 : 3

	NAME	DATE
DRAWN	JM	2/1/22
CHECKED	SV	2/2/22
ENG APPR.	BW	2/5/22
MFG APPR.	CD	2/6/22
Q.A.	JJ	2/7/22

COMMENTS:

Unit: Inches

UNLESS OTHERWISE SPECIFIED:

Payload Arrangement

TITLE: Rude Goose

SIZE	DWG. NO.	REV
B	DBF_2022_WPI_Drawing 1	

SCALE: 1:8 SHEET 1 OF 1